Structural Analysis of a Temporary Shelter with Shape Memory Effect

Ana Rita Carvalho Lopes da Silva

U. PORTO

FEUP FACULDADE DE ENGENHARIA
UNIVERSIDADE DO PORTO

Dissertation for the Master Thesis

Supervisor: Prof. António Torres Marques

Co-supervisor: Prof. Marco Parente

Mestrado Integrado em Engenharia Mecânica

September 2020

Resumo

Esta dissertação estuda uma solução de abrigo temporário previamente desenvolvida, que se caracteriza por uma estrutura origami impressa num polímero com memória de forma ativado por temperatura — DiAPLEX MM45-20. Uma solução de alojamento que seja de rápida e fácil montagem é essencial para as pessoas que perdem as suas casas repentinamente.

Realiza-se uma investigação profunda acerca de alojamento temporário, desde os abrigos mais comummente usados aos mais recentes e inovadores, as suas características, vantagens e limitações.

Várias organizações humanitárias trabalham nesta área e definem guias e requisitos para o desenvolvimento de abrigos, que podem ser consultados em documentos como o *The Sphere Handbook*.

Uma revisão literária do DiAPLEX MM45-20 revela a necessidade de caracterizar o material para determinar o seu Módulo de Young, bem como para avaliar a influência que a direção de impressão tem nesta propriedade. Este material possui um efeito de memória de forma, o que significa que o abrigo poderá ser compactado para o transporte e, posteriormente, aquecido à temperatura de 45°C, voltando à sua forma inicial.

Para validar o abrigo previamente desenvolvido, as cargas aplicadas (peso próprio, vento, chuva e neve) são calculadas, de acordo com o Eurocódigo.

Através do Método dos Elementos Finitos e do *software* ABAQUS ®, várias soluções foram analisadas — material reforçado com fibra, adição de pilares, reforço com barras e estrutura sandwich — de forma a verificar o requisito de rigidez imposto pelo Eurocódigo, tendo também em consideração a massa final do abrigo.

A estrutura sandwich revela-se uma solução promissora e, consequentemente, é realizada uma análise de sensibilidades para obter a solução ótima para aplicar no abrigo.

Palavras-chave: polímero com memória de forma, abrigo temporário, análise estrutural, método dos elementos finitos

Abstract

This dissertation studies a previously developed sheltering solution, characterized by an origami structure printed in a shape memory polymer activated by heat — DiAPLEX MM45-20. A fast and easy-assembly shelter is essential to displaced people that suffer from loss of their house.

A thorough investigation on temporary housing was held. From the most commonly used shelters to newly developed ones, their characteristics, advantages and drawbacks were analysed.

Humanitarian organizations establish guidelines and requirements for temporary shelters in documents such as *The Sphere Handbook*.

A review on DiAPLEX MM45-20 showed the need for a material characterization to determine the Elastic Modulus, as well as to understand the influence of the printing direction on this property. This material shows a shape memory effect, which means the shelter can be closed for transportation reasons and then, later on, heated to 45°C and it will deform back to its initial shape.

In order to validate the shelter previously developed, the loads applied to the shelter were calculated according to the Eurocode: overload, self weight, wind and snow.

Afterwards, using the Finite Element Method and ABAQUS ®, several solutions — reinforced material, addition of pillars, reinforcement with a skeleton of bars and a sandwich structure — were analysed with the goal of achieving the requirement defined by Eurocode in terms of maximum displacement, having in mind the shelter's mass.

The sandwich structure solution is the most promising one and, consequently, a sensitivity analysis was performed in order to understand how to achieve the optimal structure to apply to the shelter.

Keywords: shape memory polymer, temporary shelter, 4D printing, structural analysis, finite element method

Agradecimentos

Ao professor António Torres Marques, por propôr este projeto e por nunca ter deixado de acreditar nele e na sua validade.

Ao professor Marco Parente, por se mostrar sempre disponível para me ajudar com as inúmeras dúvidas e dificuldades que foram surgindo.

Ao Laboratório de Desenvolvimento de Produto e Servicos, e em particular ao Bruno Areias, que além das impressões necessárias ao desenvolvimento desta tese, partilhou comigo o seu tempo, esforço e conhecimento acerca de materiais, impressão 3D e até Estatística.

Ao professor Miguel Figueiredo, do Laboratório de Ensaios Tecnológicos, pela realização dos ensaios de tração e pelo conhecimento transmitido.

Ao professor José Luís Esteves, que numa fase inicial foi essencial para desmistificar a complexidade da estrutura.

À minha família, que sempre me apoiou mas que nunca me vai pedir para projetar esgotos e ares condicionados.

E aos que me mostraram ao longo destes cinco anos que com um bocado de tristeza também se faz um samba.

Contents

Nomenclature

Abbreviations

AVA	*Accompanying Variable Action*
BVA	*Base Variable Action*
CAD	*Computer-aided design*
Core H	*Hexagonal core*
Core Q	*Quadrangular core*
Core RH	*Horizontal recess core*
Core RV	*Vertical recess core*
Core T	*Trellis core*
DDM	*Direct Differentiation Method*
DSA	*Design Sensitivity Analysis*
FDM	*Fused Deposition Modelling*
FEM	*Finite Element Method*
FEUP	*Faculdade de Engenharia da Universidade do Porto*
FGF	*Fused Granular Fabrication*
HDPE	*High density polyethylene*
IFRC	*International Federation of Red Cross and Red Crescent Societies*
IOM	*Internation Organization for Migration*
LDPE	*Low density polyethylene*
PA	*Permanent Action*
PES	*Polyester*
PLA	*Polylactic acid*
PTFE	*Polytetrafluoroethylene*
PU	*Polyurethane*
PVC	*Polyvinyl chloride*
SiC	*Silicon Carbide*
SM	*Shape Memory*
SME	*Shape Memory Effect*
SMP	*Shape Memory Polymer*
SMPC	*Shape Memory Polymer Composite*
STR	*Structural*
UNHCR	*United Nations High Commissioner for Refugees*
UV	*Ultraviolet*

Symbols

T_g	Transformation temperature, Transition temperature — °C
E	Elastic Modulus, Young's Modulus — Pa
b	Width of specimen — m
h	Thickness of specimen — m
σ	Stress — Pa
F	Measured force — N
S	Cross-sectional area of specimen — m^2
α	Confidence interval — %
$\boldsymbol{u}$	Local displacement vector — m
$\boldsymbol{\varepsilon}$	Strain vector
$\boldsymbol{\sigma}$	Stress vector — Pa
$\boldsymbol{D}$	Elasticity matrix
G	Shear Modulus — Pa
ν	Poisson coefficient
V	Shell volume — m^3
A	Area of shell surface — m^2
$\boldsymbol{t'}$	Surface load vector — N
$\boldsymbol{p'}$	Concentrated and distributed loads vector
n	Number of nodes of element
N_i	Shape function
x,y,z	Cartesian coordinates
ξ, η	Parametric coordinates
$\boldsymbol{B}$	Strain matrix
$\boldsymbol{K}$	Stiffness matrix — N/m
$\boldsymbol{f}$	Equivalent nodal force vector — N
$\boldsymbol{a}$	Global displacement vector — m
$\boldsymbol{T}$	Transformation matrix
ϕ_a	Design response
h_b	Design parameter
q_k	Uniformly distributed overload — N/m^2
Q_k	Concentrated overload — N
q_p	Peak dynamic pressure — N/m^2
I_v	Air turbulence
ρ	Air density — kg/m^3
v_m	Wind's average speed — m/s
k_I	Turbulence coefficient
c_o	Orography coefficient
z_0	Roughness length
z_{min}	Structure's minimum height — m
z_{max}	Structure's maximum height — m
c_{pe}	Exterior pressure coefficient
c_{pi}	Interior pressure coefficient
$c_{p,final}$	Final pressure coefficient

w_{final}	Final wind pressure — N/m^2
s	Snow load — N/m^2
μ_i	Snow's shape coefficient
C_e	Exposure coefficient
C_t	Thermal coefficient
s_k	Snow load characteristic value — N/m^2
d	Diameter — m
t	Thickness — m
E_c	Young's Modulus of core — Pa
E_h	Young's Modulus of material of wall of core — Pa
t_h	Thickness of wall of core — m
l_h	Length of angled wall of core — m
$(EI)_{eq}$	Equivalent stiffness — Nm^2
I_c	Moment of inertia of core — m^4
E_s	Young's Modulus of material of sheets — Pa
I_s	Moment of inertia of sheets — m^4

List of Figures

List of Tables

Chapter 1

Introduction

1.1 Motivation

The aim of this dissertation is to analyse, validate and improve the solution for a shelter developed in a previous dissertation completed at FEUP. This solution is based on an origami-structure that uses a shape-memory polymer activated by heat and it is to be manufactured by what is called, generically, 4D printing. For the development of this shelter, geometrical, mechanical and structural aspects need to be simultaneously focused on, while preferably imposing minimal effort and technical knowledge for its deployment by the displaced users [2].

The previous project was developed because there is a need for shelters that can provide a fast and easy assembly after a crisis, since current shelters either take a long time to build and/or need people with technical knowledge to build them [1]. The objectives for that shelter were for it to be practical, cost-effective, fast construction, sustainable and reusable [1].

Origami engineering is the practice of creating 3D structures through folding operations applied initially to two-dimensional entities and it has the potential to impact a big number of design and manufacturing areas [3]. The advantages include compactly stored deployable and reconfigurable structures as well as reduced manufacturing complexity [3, 4]. Foldable structures are receiving increasing attention in Mechanical Engineering and Architecture even if the kinematics and structural behaviour of the models is complex to analyse [5]. The ultimate goal with this technique is to develop a shelter that is stiff, yet foldable [6].

A transformable structure joins the well-known three-dimensional space with a fourth dimension: time. This means that it can be relocatable, reusable and mobile, having a low impact on site and, consequently, being ecologically favourable

[7]. The structure has the ability to transform from a compact, small and closed configuration to an expanded, larger and open one. Usually, this process can be reversed and repeated [7]. Deployment or unfolding is the shape transformation from a compact configuration to an expanded, operational one, while retraction or folding is the reverse process [8]. The behaviour of the structure during these processes is as important as the behaviour under service [8].

Solutions based on modularity and deployability are desirable since those characteristics provide compactness, ease of storage and transportation and reuse [2]. Modularity is the capability of repeating units to form expanded structures, while deployability means being able to fold or package a structure into small volumes that will later be expanded to a larger size for utilization [2].

It is important to state that this project follows the restrictions and rules imposed by organizations such as the International Organization for Migration (IOM) and the *Sphere* Association, and that it concerns a first emergency shelter, not a permanent one [1]. However, in the aftermath of a disaster, the main response by governments and humanitarian organizations is the distribution of tents or sheltering kits with basic materials and tools. These solutions are meant to be short-term, but that is not what happens in a lot of cases. The 2010 Haiti earthquake (in January) is an example of this issue: in the four months after the disaster, approximately 752 000 basic shelter items such as tents and tarpaulins were distributed, but many families remained living with poor shelter during 2010 and even the following years [9].

Although humanitarian organizations are usually quick to take action, a lot of people are still not receiving help when it comes to housing. If locals had immediate access to an emergency shelter, diseases and death rates would certainly be reduced [10]. In addition, this is a concept that could be included in an emergency kit, providing not only a shelter that is quick and easy to assemble, but also replacement for the tarpaulin: something to provide structure and, at the same time, cover [1].

The developed shelter can be applied to numerous situations, from crisis originated from natural disasters to homelessness. Homelessness can expose people to the weather, crime, unsanitary conditions and damage mental health. This shelter could provide housing so that people have the conditions to find a job and rebuild their lives. It is proven that housing and its design can help families to find the head space to get employed and improve their relationships. This translates as more positive and active people in our society [11].

1.2 Objectives and structure

The main goal of this dissertation is to analyse and improve a temporary shelter. In order to accomplish this, several subgoals are imperative, such as:

- Understanding of the area of temporary housing and its current condition;
- Characterization of DiAPLEX MM45-20;
- Calculation of the loads applied to the shelter;
- Static analysis of several solutions;
- Improvement of shelter.

The content of this dissertation is divided in eight chapters. In **Chapter 1**, it is introduced the need for this research and it is explained the previous work that culminated in the shelter here analysed.

Chapter 2 refers some of the most important humanitarian organizations that work towards helping displaced people in terms of housing. Then, examples of temporary shelters are detailed: from the most common ones (tents and tarpaulins) to the most recent and innovative ones developed.

Chapter 3 explains the theoretical concept of shape memory effect in polymers. It describes DiAPLEX MM45-20, stating some properties and detailing the process of characterization through tensile testing several printed specimen. This chapter ends by showing how shape memory polymers' properties can be enhanced.

In **Chapter 4**, an introduction to 3D and 4D printing is done, and it is detailed how DiAPLEX MM45-20 is printed.

In **Chapter 5**, the theoretical concepts related to the Finite Element Method and Sensitivity Analysis are explained.

In **Chapter 6**, the loads applied to the shelter are calculated and the structural requirements are presented.

Chapter 7 analyses the results from the simulations performed, comparing several solutions. In the end of the chapter, a sensitivity analysis on a sandwich structure is performed.

Finally, **Chapter 8** presents the final conclusions as well as recommendations for future work.

1.3 Previous work

The shelter previously developed can be seen in Figure 1.1. Its area is approximately 10.4 m^2 and it is 2.6 m high, with a door opening 1.8 m high. This is idealized to provide shelter for 2 to 3 people. It was also suggested the combination of two shelters, thus providing living space for bigger families. This is achieved using models with two openings in order to connect them [1]. Appendices A, B and C show the technical drawings of the shelter without any doors, with one door and with two, respectively.

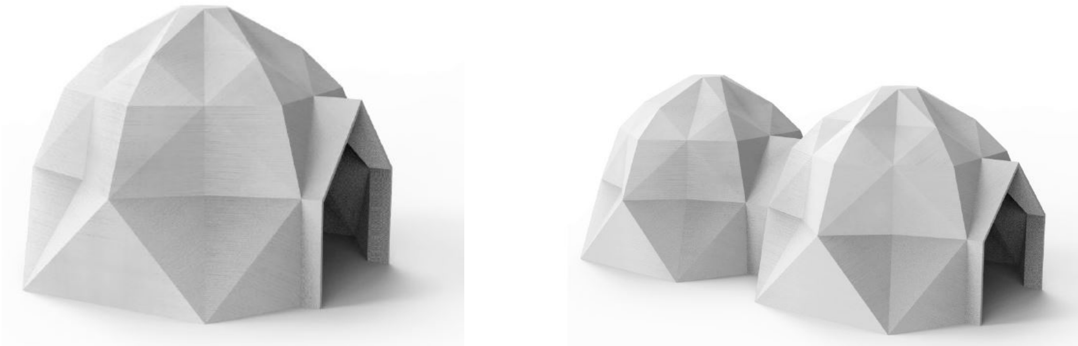

Figure 1.1 Shelter previously developed: a basic unit and a configuration with two modules [1].

In large scale applications, the Fused Granular Fabrication (FGF) process using SMP pellets would reduce the cost of production of the shelter. At industrial scale, the cost would be approximately 2256 euros per shelter (1.5 mm thickness and 45.8 kg) [1]. This is a solution for a shelter that has in mind several issues: being built in a short amount of time, without the need for technical knowledge or other materials, having enough space for a family and having the possibility of joining several units [1]. However, it did not have in mind other issues, such as the structural integrity and durability of the shelter, considering the climate and the unfolding, as well as its thermic and acoustic insulation [1].

Summarizing, the requirements that were previously successfully validated can be seen next [1]:

- Have a minimum of 3.5 m^2 living space per person and at least 2 m height.
- Consider the reusability and sustainability of the material.
- Support family shelter over common one.
- Provide assistance and material for displaced people to build on their own.

- Be adaptable or modular in order to fit the emergency kit dimensions and shipping sizes in pallets (120x110 cm^2).
- Weigh no more than 50 kg.

However, some requirements were not achieved or not tested [1], such as adapting the shelter to climate conditions and geographical context, testing and validating the material according to the standards provided by humanitarian organizations and accomplishing a cost of less than 270 euros.

It was suggested the previous research would be further developed following some recommendations [1]:

- Analyze and characterize the mechanical properties of the material (SMP filament and SMP pellets).
- Determine how to hold the structure to the different types of soil.
- Study the attachment of the door to the rest of the structure.
- Test the models for several climate conditions, as well as UV test and fire retardant test.
- Simulate the process of shape memory effect from a designed concept, in order to predict the shape that the concept should be printed and, later on, folded and restored.
- Estimate the durability of the shelter.
- Improve the concepts design in order to facilitate the printing process that might display some challenges at large scale in the walls angles bigger than 45°, needing support structures.
- Improve the material properties in terms of specific strength, stiffness and toughness by using composite materials, for example.
- Study the possible effect of creep or relaxation in the shape-memory process.
- Consider the possibility of developing a composite material from SMP matrix, reducing the weight and cost of the developed structure.
- Develop a real scale functional prototype using FGF method, to validate the concept within the requirements imposed, and be accepted by humanitarian organizations, such as IOM, in order to use developed shelter after crisis situations.

Chapter 2

Shelters

2.1 Humanitarian organizations

Immediately after disasters, shelter and non-food items can be life-saving and critical for the safety and protection from the weather and health risks of the affected population. Housing assistance will always be a stabilizing influence on post-crisis population [12]. There are a lot of humanitarian organizations that can provide this assistance, as well as technical guidelines for other professionals to develop shelter solutions. Among them are the International Organization for Migration, the International Federation of Red Cross and Red Crescent Societies, the United Nations Refugee Agency and the *Sphere* Association.

The **International Organization for Migration** (IOM) assists in resolving the challenges of migration management, as well as understanding migration issues and uphold human dignity and well-being of migrants [13]. It specifically plays a major role in shelter operations worldwide. During 2018, IOM's Shelter program reached around 4 million people across 44 countries, by either assisting them financially, providing and repairing shelters or giving shelter training [14].

The **International Federation of Red Cross and Red Crescent Societies** (IFRC) was founded more than a century ago and is currently one of the largest humanitarian organizations as it provides assistance to everyone in need, regardless of nationality, race, class or religion. This organization works in four main areas: promotion of humanitarian values, disaster response, disaster preparedness and health and community care. Specifically, it is involved in providing solutions for shelter to displaced people such as tents, shelter kits or materials to build/repair homes [15]. These shelter kits are a flexible, fast and cheap solution that contain a set of tools and fixings, as well as two plastic tarpaulins. Eventually, the shelter built can be upgraded [16]. In the present chapter, this solution will be further explained.

The United Nations High Commissioner for Refugees (UNHCR), or the **United Nations Refugee Agency**, is a global organization that dedicates to protecting refugees and forcibly displaced and/or stateless people. This organization works closely with IFRC, but while the former deals with conflict generated situations, the latter covers displacement caused by natural disasters.

Lastly, the ***Sphere*** **Project** originally was created by the Red Cross and the Red Crescent Movement with the goal of developing universal standards in core areas of humanitarian response such as Water supply, Sanitation and hygiene promotion, Food security and nutrition, Shelter and settlement and Health, in order to improve their quality in crisis situations. Eventually, in 2016 this project became an association that has revised and published several editions of *The Sphere Handbook*, which has developed into one of the most widely referenced humanitarian resources in the world and contains ethical, legal and practical guides for humanitarian response [17]. This *Handbook* clearly states two important guidelines for shelters, among many others [17]:

- Minimum of $3.5\,\mathrm{m}^2$ of living space per person;

- Internal floor-to-ceiling height of at least 2 m (2.6 m in hot climates) at the highest point.

2.2 Types of shelters

The need for sheltering can come from various reasons, such as the occurrence of a natural disaster. These can be categorized in three phases: the pre-disaster phase, the disaster/impact one and, finally, the post disaster and reconstruction phase. Each disaster, from earthquakes and floods to megafires and hurricanes, causes different types of destruction and of different intensity [2]. Shelters need to be adequate for each type of crisis and phase.

Shelters can be classified in four different types [2, 18]:

- **Emergency shelters** are meant to be used for brief periods of time (a single night to a few days) as they are the most basic kind of support;

- **Temporary shelters** are tents or mass shelters that displaced people should only use for a few weeks after a disaster;

- **Temporary houses**, on the other hand, constitute shelter for long term periods (from six months to three years) and can be rental houses or prefabricated units;
- **Permanent houses** can be upgraded from transitional houses and should be resistant to future disasters.

A shelter and a house have different purposes because shelters are only supposed to offer a safe area to live in immediately after a disaster, whereas a house includes household responsibilities [18], such as a kitchen.

The shelter analysed in this dissertation is inserted in the category of Transitional Shelters (Figure 2.1), which can be located between Temporary Shelters and Temporary Housing, since they can be disassembled, upgraded, reused, relocated and recycled, offering the potential to provide shelter for families and also facilitate personal, social and economic recovery [9], but without providing all aspects of a traditional house, such as toilet, kitchen or even ventilation. Therefore, it is not advisable for these shelters to be used permanently.

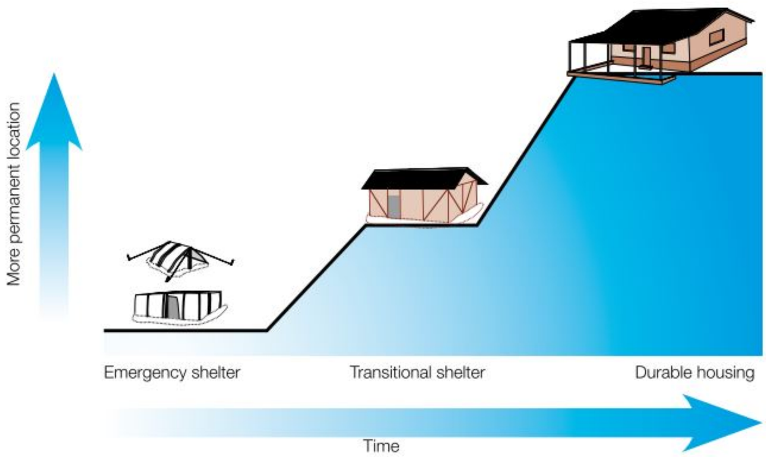

Figure 2.1 Types of shelter [19].

Nowadays, most shelters require people to use local materials. On one hand, this can be positive as it helps the local economy and manufacturers. But on the other hand, the construction of shelters becomes dependent on the quality and availability of material on the spot as well as the easiness to get it [1]. This aspect also affects the speed of the shelter's construction.

There are numerous shelters on the current market, with many different characteristics, purposes, advantages and limitations. Next, some will be described so that they can be better understood.

Shelter Kit and Tarpaulin This solution constitutes relief to the biggest number of displaced people in the least amount of time. In the long run, not an effective solution since it is very vulnerable [20]. However, it is cost effective and a simple solution. The most widely used shelter kit is provided by IFRC and is a collection of tools (rope, handsaw, nails, shovel, hoe, machete, shears, tie wire, claw hammer and woven sack) and two plastic tarpaulins (made of HDPE black fibers fabric laminated on both sides with LDPE coating). As shown in Figure 2.2, the way the kit is used can vary according to the emergency, necessity, environment, skills and local available materials [16].

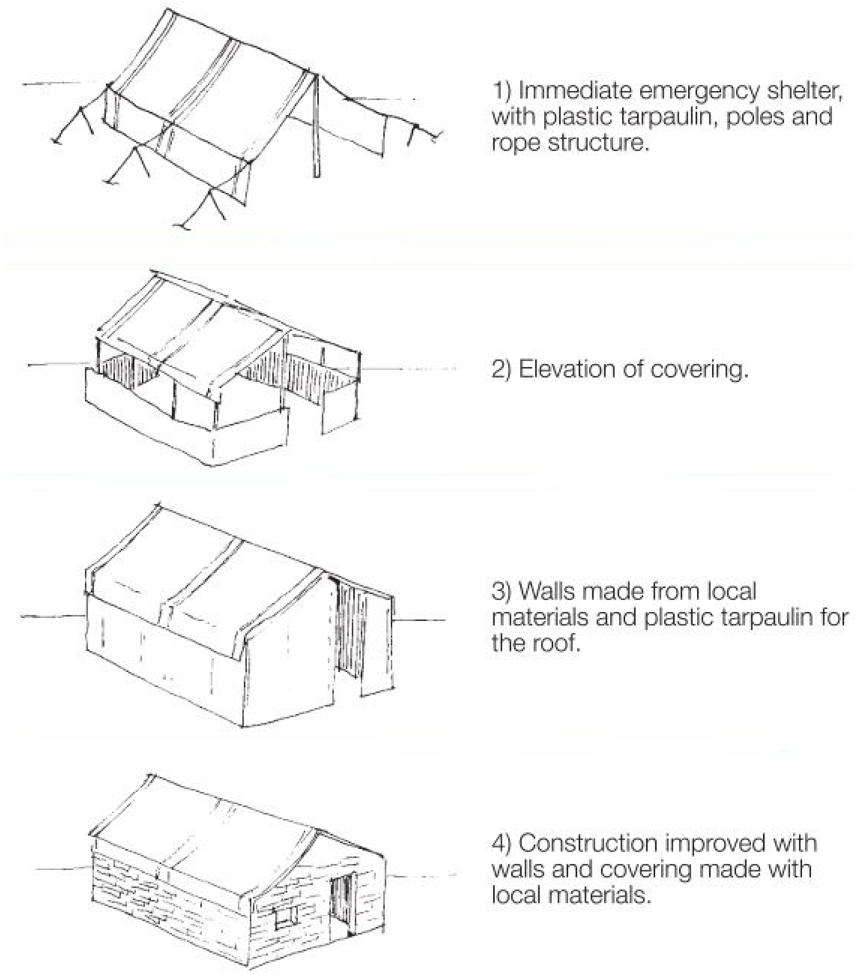

Figure 2.2 Schematic representation of possible upgrades of a shelter built with the IFRC shelter kit [16].

Tent Rigid frame with a flexible cover usually made of plastic or cotton fabric. They can be easily transported and manufactured and are more resistant than the previous solution [20]. The *Framed Tent* used by UNHCR (Figure 2.3) is to be used in urban areas and is suitable for families of five people for around one year [21]. This shelter withstands 75 km/h winds, is waterproof and gives protection

Figure 2.3 UNHCR Framed Tents [21].

against dust, wind, snow and insects when closed. Figure 2.4 shows how four tents are transported (each tent weighs about 80 kg) [21].

Figure 2.4 Transportation of four Framed Tents [21].

Next, a few non-traditional shelters will be detailed.

TornadoPod In 2016, this shelter (Figure 2.5) was tested to protect up to six people from a tornado situation. It is half buried and on top it has a sliding door to open after the disaster ends. The base is threaded so it acts as an anchor on 5400 kg of concrete. The exterior is a domed steel cage with a ballistic shield. This shield is 9.5 mm thick and consists of multiple layers of woven glass fabrics and Innegra fabrics. This is a shelter used during the impact phase of a disaster.

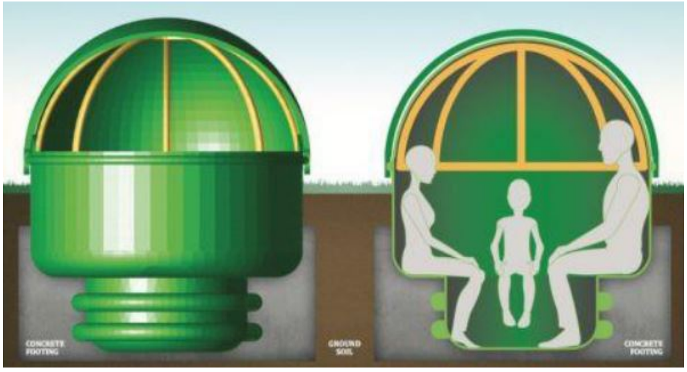

Figure 2.5 TornadoPod [22].

Big Green Box This shelter (Figure 2.6) was developed for the New Zealand's Antarctic research station. It withstands extreme weather conditions such as 200 km/h winds and temperatures of 60 °C. The unit is 8.2 m × 3.2 m × 2.7 m and its walls are made of fire-retardant, fiberglass reinforced polyurethane [23].

Figure 2.6 Big Green Box [23].

Cardborigami Made to help homeless people in Los Angeles, this shelter uses cardboard because of its insulative properties, recyclability, lightweight and higher structural integrity (when compared to a general tent). The material is treated to be water resistant to light rain. Because of the origami design, it can be instantly opened and closed as a backpack (it weighs almost 8 kg). One shelter (Figure 2.7) has space for two adults [24].

Figure 2.7 Cardborigami [24].

Designnobis' Tentative A compact living space (Figure 2.8) for two adults and two children that can be deployed in any climate/terrain and consists of a textile with insulating perlite sandwiched between layers and held by an aluminium frame. The roof collects water and provides ventilation, while the floor is above ground and made out of heat-insulating recyclable composite decks. For transportation, the shelter closes and becomes 4 m × 2 m and 30 cm tall [25].

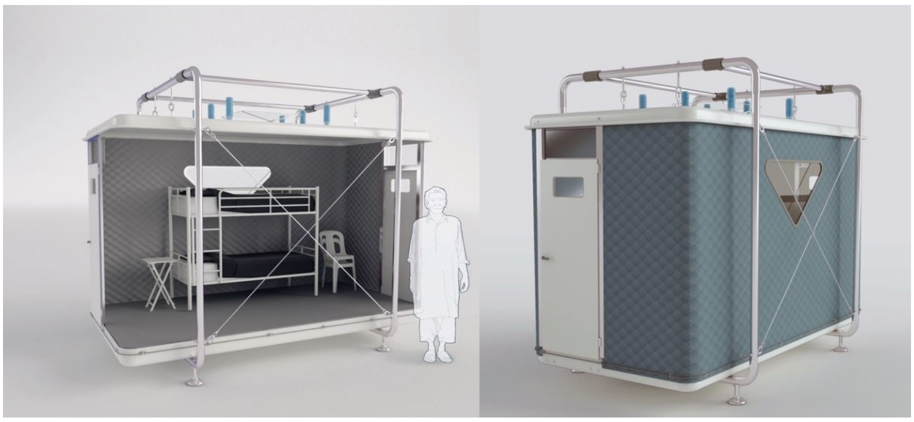

Figure 2.8 Designnobis' Tentative [25].

Just A Minute This temporary shelter can be compared to an accordion when it opens and closes (Figure 2.9). The central core is made of bamboo, as well as the window shaders and floor panels. The windows' material is polycarbonate and the recycled wool is added to provide insulation. It is a modular solution [26].

Figure 2.9 Just A Minute [26].

SheltAir A pavilion developed in Berlin with an elastic gridshell and a pneumatic falseworks in the form of air-filled cushions made of PVC-coated polyester. It uses minimal material and takes eight hours to inflate, without the need for substantial physical work. This shelter (Figure 2.10) accommodates more that one family, but can be adapted to different sizes [27]. It was recently used to isolate COVID-19 patients.

Figure 2.10 SheltAir [27].

Fold&Float This foldable structure (Figure 2.11) was developed to be used in Istanbul in the case of an earthquake taking place, since all the former public spaces set aside for emergency situations are now privatized. It is made out of light steel and is 21 m^2. It has an upper structure with folded furniture and a floating pontoon of concrete [28].

Figure 2.11 Fold&Float [28].

Weaving A Home This structural fabric shelter (Figure 2.12) collapses into a flat surface for transportation and can adapt to a number of climates. As can be seen in detail in Figure 2.13, it is constructed with high-strength plastic tubing woven into a stretchable fabric membrane. The structure can be altered, opening segments to create doorways or windows, or closing them to keep the heat inside during cold months. The tubing provides conduits for electricity and water and there is a water tank on top of the dome that collects rain water through thermosiphoning [29].

Figure 2.12 Weaving A Home [29].

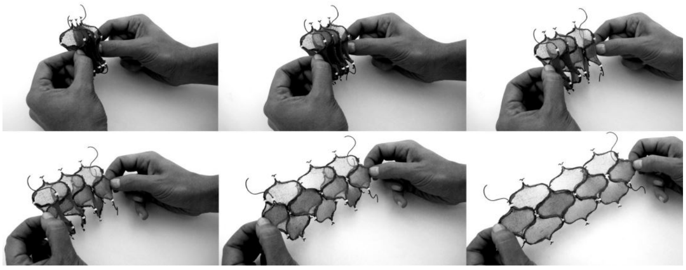

Figure 2.13 Weaving A Home - fabric [29].

Shelter Squared The goal of this design is to give privacy to families on a post disaster situation when they live in big shared spaces such as gymnasiums or pavilions (Figure 2.14). When closed and flat, it becomes the size of a mattress and takes 15 minutes to assemble. The shelter is composed of waterproof panels and recyclable materials [30].

Figure 2.14 Shelter Squared [30].

Maidan Tent This structure allows for a place where the community can come together and interact (Figure 2.15). It is made of aluminium and covered by a textile composed of 20% PU and 80% PES (resistant to water, winds of 110 km/h and fire). The tent has eight semi-private spaces, that can be used for several different activities [31].

Figure 2.15 Maidan Tent [31].

Chapter 3

Shape memory materials

Shape memory materials are stimuli-responsive materials that have general characteristics of low density, large deformation, variable stiffness, adjustable transition temperature, low impact during deployment, biocompatibility and biodegradability [32, 33]. The deformation of these materials is driven by a shape memory effect.

It is important to distinguish shape **changing** materials from shape **memory** materials. The former change their shape immediately when the stimulus is applied and recover the original shape immediately after the stimulus is removed. This means this type of materials can't maintain a temporary shape, as opposed to shape memory materials [34].

Shape memory materials can be divided into several categories, such as shape memory alloys, shape memory polymers (SMP), shape memory hybrids, shape memory ceramics, shape memory polymer composites (SMPC) and shape memory gels [35]. For the purpose of this dissertation, SMP are the main focus. At the end of this chapter, SMPC are mentioned, since they can improve the material's properties.

3.1 Shape memory polymers

Shape memory polymers are defined as polymeric smart materials that offer mechanical action triggered by an external stimulus. This means they can recover from a deformed temporary shape (or multiple) to their original one through the application of an external stimulus, such as temperature, magnetic fields or light [36, 37]. This is achieved by material immobilization, commonly vitrification or crystallization [38]. This functionality is called shape memory effect (SME) [39]. SME, rather than a material property, is a response given by the material under a set of loading conditions [33].

According to its stimulus, SMP can be divided into thermal-sensitive, light-induced, electroactive, ph-sensitive and magnetic-induced materials [32]. In this dissertation, the process of a thermal-sensitive SMP will be studied, since the material used for the development of the shelter is stimulated by temperature. Accordingly, thermal-responsive SMP respond to temperature, thus being the most prospective materials because of the simple stimulus form and fast response [40].

The SM cycle is the evolution of stress, strain and temperature during thermo-mechanical cycling of an SMP [38]. The process (Figure 3.1) can be divided in three basic stages [32, 38]:

1. **Heating and Shaping:** initially, the material is deformed into a desired temporary shape under external load after being heated to at least its transformation temperature (T_g);

2. **Cooling and Fixing:** as the external load is maintained and the temperature lowered (below transition temperature), the sample adopts a more rigid state and immobilizes the polymer chains, fixing the deformation. Upon unloading, the shape stays unaltered.

3. **Reheating:** afterwards, the original shape can be restored by heating the material without any stress to a temperature higher that the temperature of transition.

This phenomenon can be better understood if further details are explained. SMP are copolymers formed by two type of segments: hard and soft ones. In the hard segment, cross links among monomers provide the elasticity and mechanical strength required for the reshaping of the material when heated above the transition temperature. These hard segments store strain energy during deformation. In turn, the soft segment maintains the shape of the part when the temperature is lower than the transition temperature. However, it loses its strength if temperature is above T_g. This means that when the mechanical deformation occurs while the temperature is higher than transition temperature, the part presents a low Young's Modulus because the soft segments have lost their stiffness - and vice versa. The original shape has certain segment chains and when stress is applied the chains are reoriented. When deformation ends, the part is cooled down and the soft segments form a new segment chain configuration by vitrification. This guarantees a fixed new shape until the sample is reheated. When that happens, the soft segments lose their strength and cannot support the new segment chain configuration. Due to entropy, the stored strain energy is released (it is energetically favourable for the material to return to its disordered conformation by releasing the stored strain energy) and the shape memory effect is triggered [39]. These materials are temperature-sensitive, which means they show different mechanical properties at different temperatures. Since they have low Elastic Modulus when the temperature is high, the strain energy decreases gradually with the increase in temperature [40].

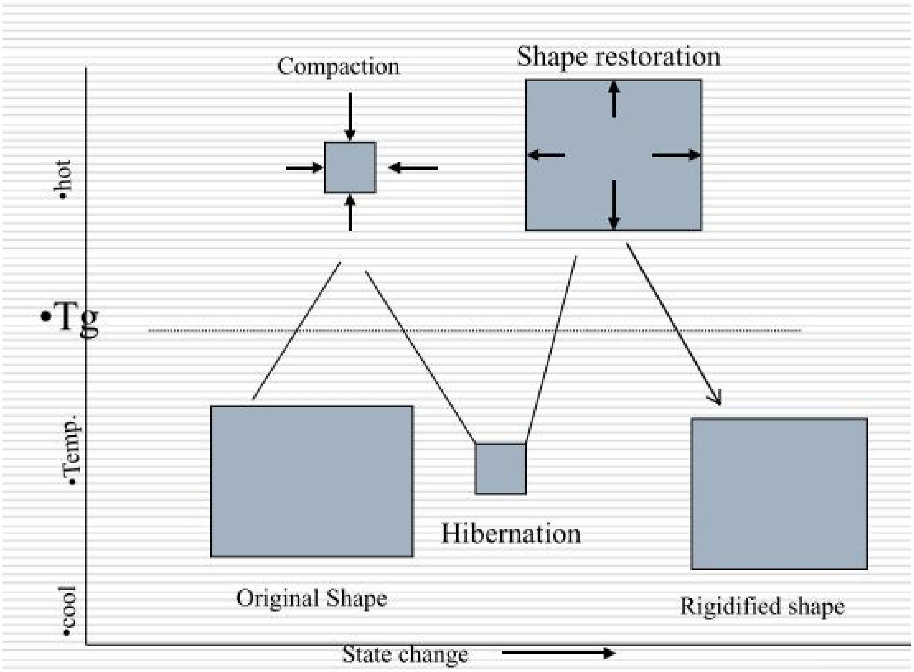

Figure 3.1 Schematic representation of the shape memory cycle [41].

The theoretical modelling of the mechanical behaviour of an SMP is not trivial, but can be used, together with simulation tools, to reproduce the SM behaviour [42]. Currently, there are two approaches to develop a constitutive model for materials with a shape memory behaviour: the linear viscoelastic theory and the micromechanical theorem of phase transformation. The former applies rheological models with time and temperature dependent parameters, as well as using the entropy elasticity of the response of amorphous polymers when temperature is high. The latter states that the material has switchable phases, in which the material has rubbery properties at high temperature and gradually changes to a glassy state when the temperature is lowered. Therefore, the SM behaviour is explained by the transition between phases. This approach is usually applied to crystallizable polymers [33, 43].

The properties of SMP are experimentally determined using a variety of techniques, such as uniaxial tensile, cyclic tensile, creep, point deflection and nanoindentation tests [44].

3.1.1 DiAPLEX MM45-20

The material used to print the shelter analysed in this dissertation is DiAPLEX MM45-20 and will be described next. It was supplied by *SMP Technologies, Inc* in the form of pellets, even though it is also available as solution, foam, microbeads and fiber [41].

The DiAPLEX SMP are newly developed intelligent materials that consist in segmented polyurethanes whose morphological structure is bi-phasic (soft phase matrix with hard phase inclusions — see Figure 3.2). They are activated by heat (above the soft phase transition temperature). These materials are used in several areas, such as medical, space exploration, clothing, food packaging and toys [45, 41].

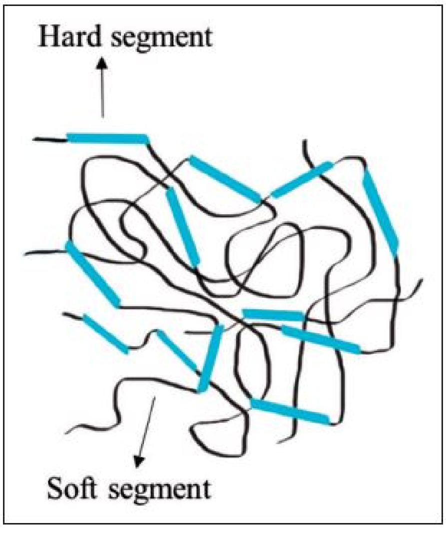

Figure 3.2 Schematic representation of a polyurethane fiber [46].

DiAPLEX has been authorized by the Japanese Ministry of Health and Welfare to be used in food-related products. In addition, it only shows high moisture permeability above the transition temperature — see Figure 3.3 [41].

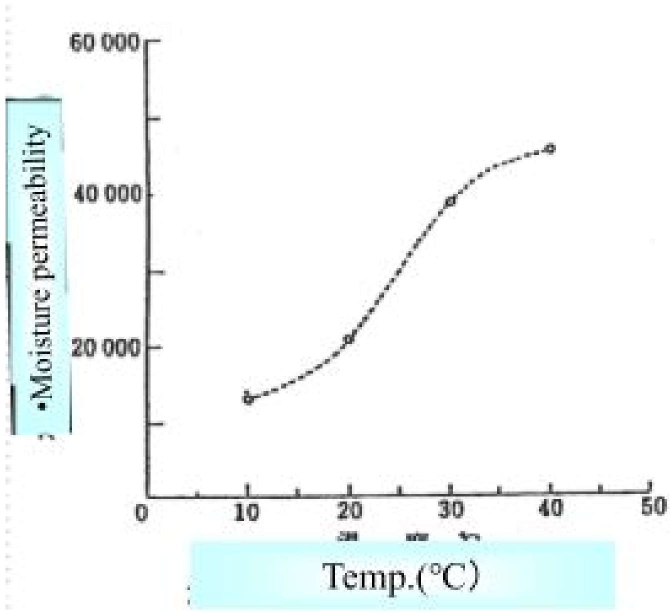

Figure 3.3 DiAPLEX's moisture permeability evolution [41].

As previously explained, the Elastic Modulus of these SMP is temperature dependent, meaning it changes largely below and above transition temperature [47]. As can be seen in Figure 3.4, below the transition temperature, the Young's Modulus (E) is higher and as the temperature increases, E decreases.

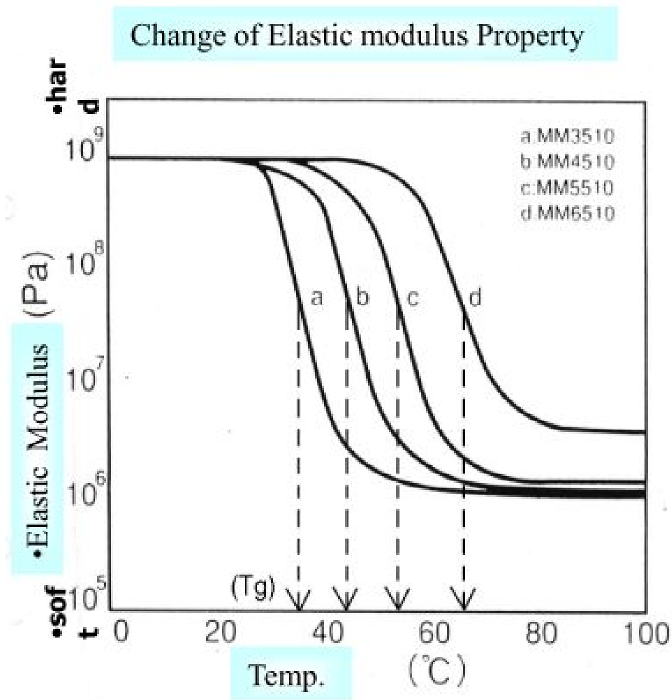

Figure 3.4 DiAPLEX's Elastic Modulus' evolution with respect to temperature [41].

Thus, Figure 3.4 shows the variation of E with respect to temperature of four different DiAPLEX materials. DiAPLEX MM45-20 is a cross-linked glassy copolymer with a transition temperature of 45°C; when temperature is lower than that value, E is approximately 1 GPa and when higher, E drops to around 1 MPa [41]. This material has a melting temperature of 200 °C [39].

When 3D printing DiAPLEX MM45-20, as will be studied in Chapter 4, it is known that the final part's Young's Modulus variation is mostly caused by printing velocity, followed by temperature and then layer height. Low velocity leads to a higher Young's Modulus, since more material is deposited along the path and, therefore, the part has better layer bonding. High temperature in processing leads to higher Elastic Modulus because it reduces the material's viscosity, it flows more easily out of the nozzle and, therefore, deposits more material [39].

3.1.1.1 DiAPLEX MM45-20 characterization

In order to validate the data provided by *SMP Technologies, Inc* (Figure 3.4), as well as determine the Young's Modulus of DiAPLEX MM45-20 considering different printing directions, a tensile test was held. Three directions were studied (0°, 45°and 90°) — see Figure 3.5.

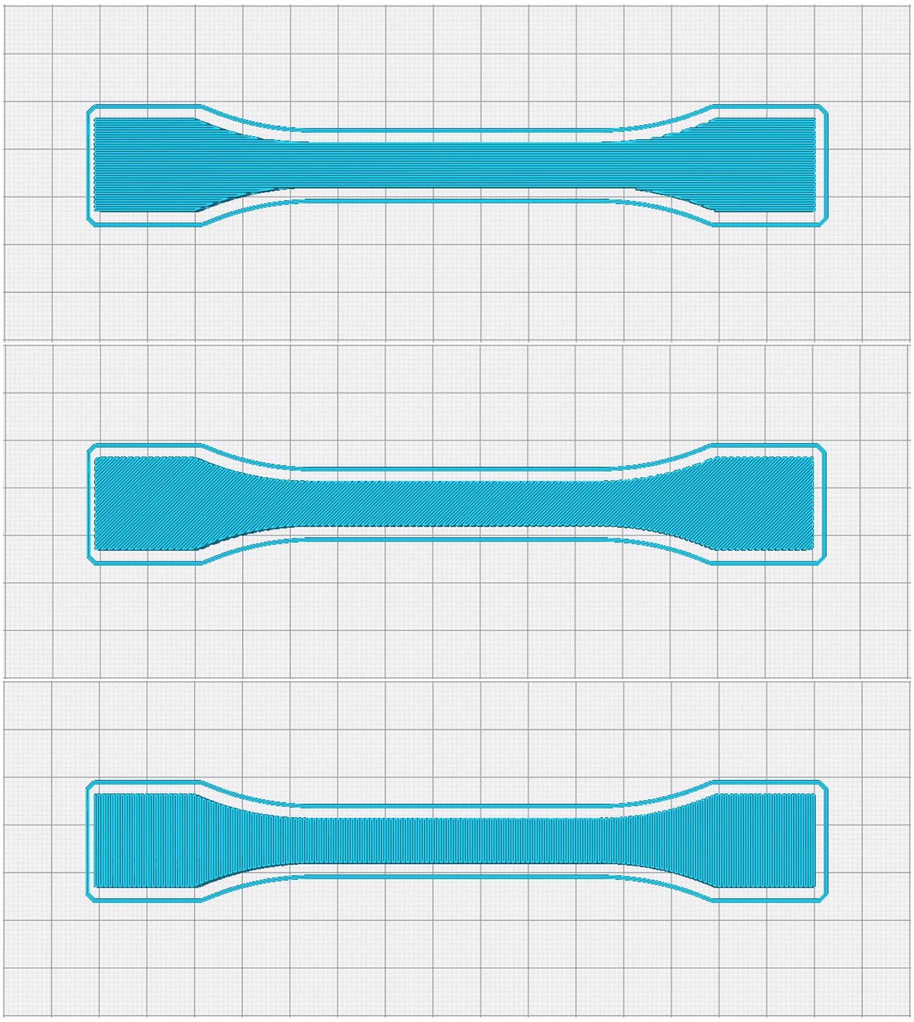

Figure 3.5 Three printing directions studied: 0°, 45° and 90°, from top to bottom.

The mass of each specimen was measured with a *HLD 300* scale (plate dimensions d = 120 mm, capacity 300 g, Standard division 0.05, HR division 0.005, linearity ±0.01 g, internal sensitivity 0.0005). The dimensions were measured with a *Mitutoyo CD-6" ASX* caliper (range 0 − 150 mm, accuracy 0.02 mm, resolution 0.01 mm, repeatability 0.01 mm). The testing machine *MTS 810* (Figure 3.6) is servo-hydraulically operated with a maximum load of 100 kN. The load was measured by an *MTS* load cell with a maximum of 10 kN. The strain was measured by a *MTS* extensometer of $L = 50\,\mathrm{mm}$ (that only reads a maximum of 50% of strain) as it was clamped to the specimen in each test.

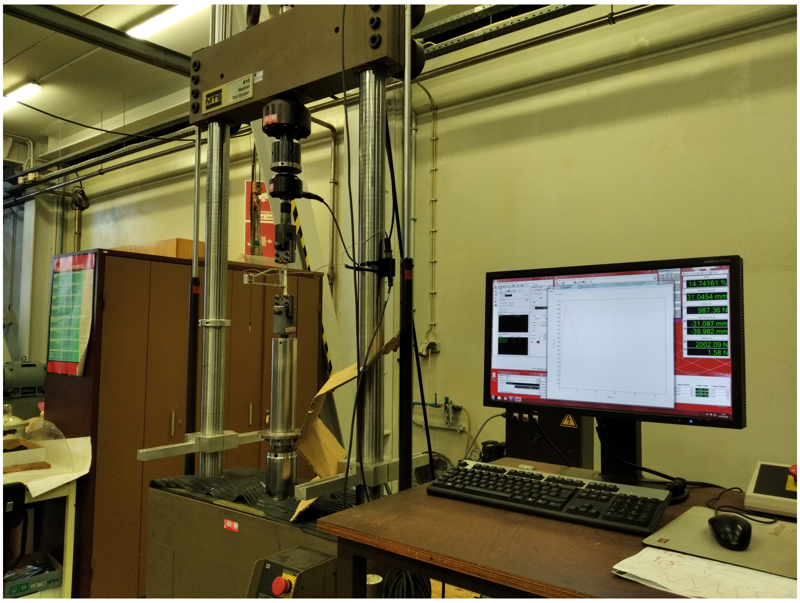

Figure 3.6 Set-up for tensile testing of DiAPLEX MM45-20.

According to *ISO 527: Plastics - Determination of tensile properties*, three specimens of 1B type (Figure 3.7) were printed in each of the three directions that were studied.

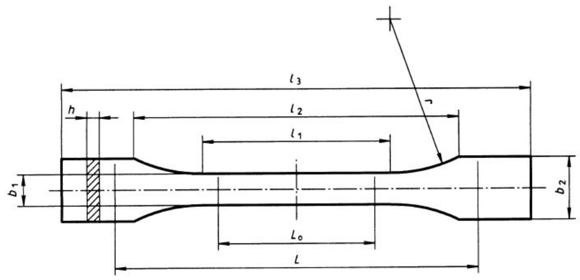

Dimensions in millimetres

	Specimen type	1A	1B
l_3	Overall length	$\geqslant 150$[a]	
l_1	Length of narrow parallel-sided portion	80 ± 2	$60{,}0 \pm 0{,}5$
r	Radius	20 to 25	$\geqslant 60$[b]
l_2	Distance between broad parallel-sided portions	104 to 113[c]	106 to 120[c]
b_2	Width at ends	$20{,}0 \pm 0{,}2$	
b_1	Width of narrow portion	$10{,}0 \pm 0{,}2$	
h	Preferred thickness	$4{,}0 \pm 0{,}2$	
L_0	Gauge length	$50{,}0 \pm 0{,}5$	
L	Initial distance between grips	115 ± 1	$l_2\,{}^{+5}_{\ 0}$

NOTE Specimen type 1A is preferred for directly-moulded multipurpose test specimens, type 1B for machined specimens.

[a] For some materials, the length of the tabs may need to be extended (e.g. $l_3 = 200$ mm) to prevent breakage or slippage in the testing jaws.

[b] $r = [(l_2 - l_1)^2 + (b_2 - b_1)^2]/4\,(b_2 - b_1)$

[c] Resulting from l_1, r, b_1 and b_2, but within the indicated tolerance.

Figure 3.7 Dimensions of type 1A and 1B specimen [48].

Figure 3.8 shows the specimens tested:

- Specimens 1, 2 and 3 — direction 0°
- Specimens 4, 5 and 6 — direction 45°
- Specimens 7, 8 and 9 — direction 90°

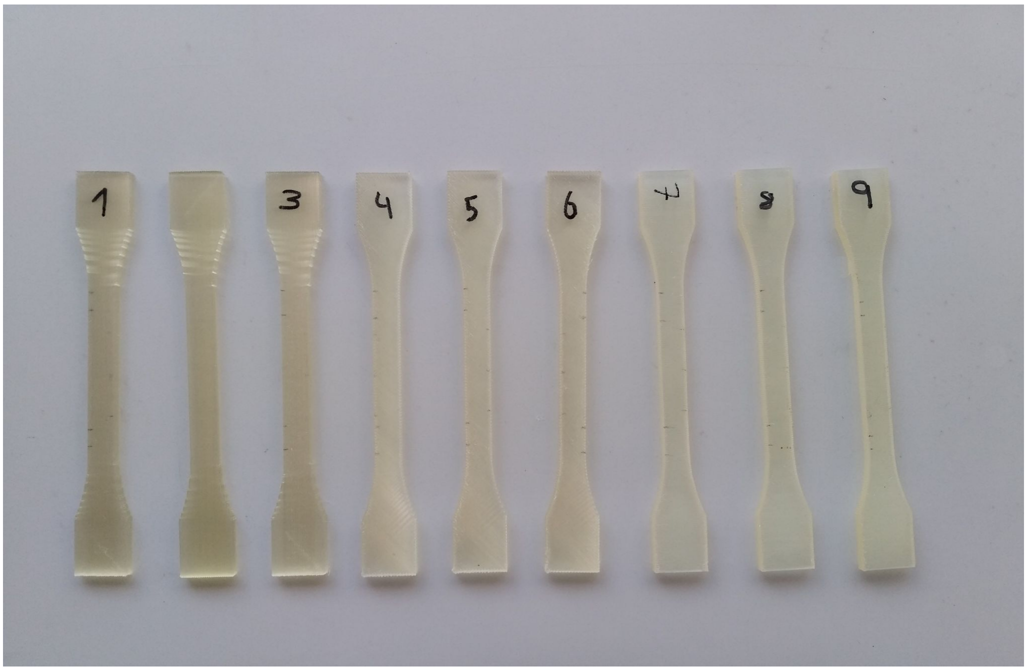

Figure 3.8 Printed test specimens.

Experimental Procedure

1. 3D printing of the specimens. The printing conditions are subsequently detailed in Chapter 4.

2. Measuring the width b and thickness h of the specimen at the center and 5 mm of each end of the gauge length. The arithmetic mean was calculated, for posterior calculation purposes. Even though the tolerances according to *ISO 527* are not satisfied, the specimens were considered valid since they were printed with a nozzle of 0.4 mm diameter, which makes it extremely hard to guarantee tolerances of 0.2 mm.

Table 3.1 Dimensions and mass of specimens.

Specimen	**Width** (mm)	**Thickness** (mm)	**Mass** (g)
1	9.71	3.85	9.33
2	9.70	4.07	9.86
3	9.74	4.00	9.78
4	9.86	4.11	9.90
5	9.93	4.26	10.03
6	9.83	4.26	10.05
7	9.76	4.20	9.96
8	9.91	4.20	9.91
9	9.81	4.15	9.86

3. The specimen was mounted on the machine and firmly clamped. The extensometer was attached to the specimen and the settings adjusted in the software. The test was initiated with a testing speed of 5 mm/min. The software showed in real-time a graph of force-% strain and recorded the values of time, force and strain in mm.

4. Step 3 was repeated for all specimens.

5. Calculations were performed in order to get the results, presented next.

Observations Only in specimens 4 and 5 the deformation and rupture happened inside the area covered by the extensometer. In this matter, all of the other tests were invalid because there was elastic recovery and, therefore, the yield properties could not be studied. However, all of the tests were valid to calculate the Young's Modulus, which was the main purpose of the experimentation.

Results According to *ISO 527*, stress (σ) and the modulus (E), both in MPa, are calculated in the following way:

$$\sigma = \frac{F}{S} \tag{3.1}$$

$$E = \frac{\sigma_2 - \sigma_1}{\varepsilon_2 - \varepsilon_1} \tag{3.2}$$

where F is the measured force (in N), S is the initial cross-sectional area of the specimen (in mm^2), σ_1 is the stress (in MPa) measured at the strain value $\varepsilon_1 = 0.0005$ and σ_2 is the stress (in MPa) measured at the strain value $\varepsilon_1 = 0.0025$. Both stress and the modulus must be calculated to three significant figures. The strain was not calculated because the values were automatically recorded by the extensometer.

Table 3.2 Elastic Modulus calculation.

Specimen	**Area** (mm^2)	**Stress** σ_1 (MPa)	**Stress** σ_2 (MPa)	**Elastic Modulus** (MPa)
1	37.38	1.46	6.55	2550
2	39.48	1.97	6.83	2420
3	38.96	1.40	6.13	2370
4	40.52	1.40	5.83	2230
5	42.30	1.45	6.07	2310
6	41.88	1.51	6.00	2250
7	40.99	1.60	6.27	2330
8	41.62	1.47	5.91	2220
9	40.71	1.37	5.74	2190

Table 3.3 *ANOVA Analysis* results with $\alpha = 0.05$.

Group	**Count**	**Sum**	**Mean**	**Variance**
Sample 0°	3	7340	2446.667	8633.333
Sample 45°	3	6790	2263.333	1733.333
Sample 90°	3	6740	2213.333	433.333

With the measured mass, the density and the theoretical volume of the specimens, a value of 2% of voids was calculated. This value is insignificant, but otherwise could be the reason the values of Young's Modulus are different than the expected values of around 1 GPa.

Finally, resorting to *Excel*, an *ANOVA analysis* was performed on the results, with the goal of evaluating whether the specimens with a direction of 0° can be confirmed as better than the others.

Let F be the ratio of variation between sample means and variation within samples and p be the area to the right of F, meaning it represents the probability of observing a result ($F_{critical}$) as big as the obtained experimentally (F). Since $F > F_{critical}$, the null hypothesis that the means are equal can be rejected and, therefore, the conclusion that at least one of the sets of specimens has a mean significantly different than the others can be stated. In order to affirm which one, a *Tukey test* was also performed. This method compares all pairs of means and identifies any difference between two means that is greater that the standard error [49]. The results are shown in Table 3.4 and Table 3.5.

Table 3.4 *ANOVA Analysis* results with $\alpha = 0.05$.

Sources	**F**	**p value**	$F_{critical}$
Between Groups	12.577	0.007143	5.143

Table 3.5 *Tukey test* results with $\alpha = 0.05$.

Group 1	**Group 2**	**lower value**	**upper value**	**p value**
Sample 0°	Sample 45°	33.026	333.641	0.022
Sample 0°	Sample 90°	83.026	383.641	0.007
Sample 45°	Sample 90°	-100.307	200.307	0.592

By analysing the lower and upper values of the confidence intervals of each combination of groups, one can state with 95% of confidence that the means of sample 45° and sample 90° are similar, in oposition to the mean of sample 0°. Therefore, printing with a direction of 0° results in parts with a higher Elastic Modulus.

3.2 Shape-memory polymer composites

The most common smart materials to be used are, in fact, SMP. But they show some limitations in terms of stiffness and strength [50]. Therefore, they can be used as a composite of SMP fiber in an elastomeric matrix [51]. SMP composites (SMPC) are used to overcome the low deformation stiffness and low recovery stress, so that improved parts can be produced, or to find new stimulation methods [33, 50]. Examples of possible reinforcements are silicon carbide (SiC), aramid, glass or carbon [52, 50]. The latter shows quality physical and chemical properties and is a good combination with polymers [50].

In fact, the shape recovery behaviour can be better in SMP composites than pure SMP. For instance, Figure 3.9 shows the result of triggering the shape recovery of samples ranging from pure PLA to PLA with 40 wt% of SiC. The images clearly show that the samples with SiC filaments recover much faster.

The spatial combination of smart materials and other material is essential to the behaviour of the part [53]. Generally, reinforcement with long-fiber filler gives the best results, followed by short-fiber and particles. However, using too much filler or filler with reinforcement too strong can lead to worse mechanical and thermal properties and most fillers can actually reduce the SME of a polymer.

In short, in most cases, using reinforcement will improve the mechanical properties at the cost of reducing the fixation and recovery rate as well as the transition temperature [50]. One solution can be printing a part in composites with hinges made of shape memory polymers, so that the memory effect is guaranteed.

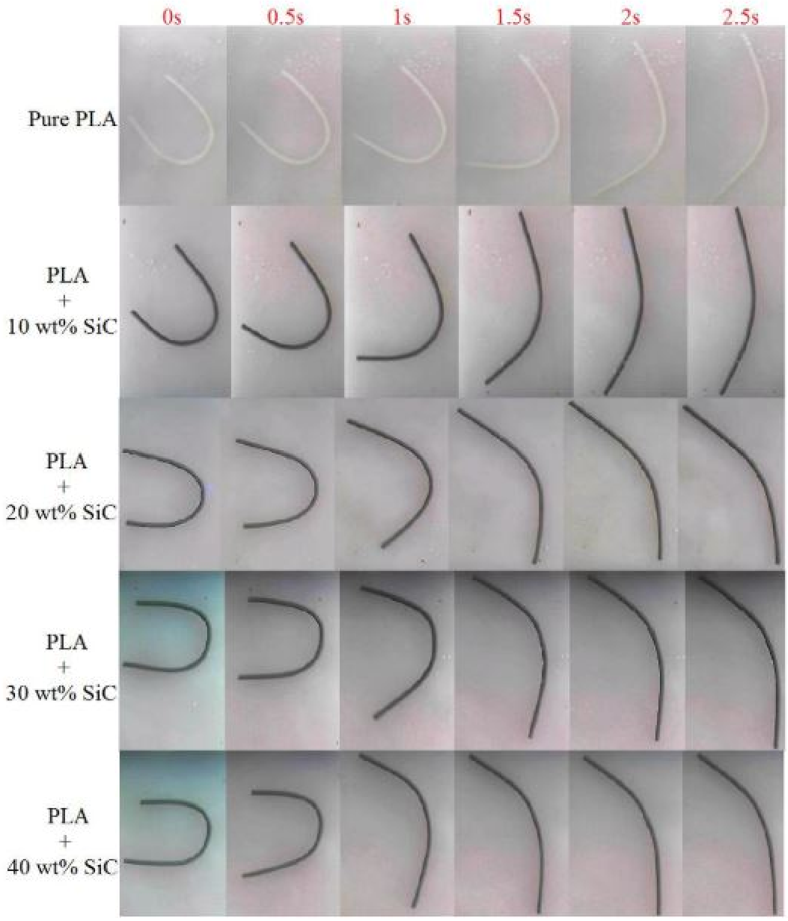

Figure 3.9 Recovery of samples of PLA and PLA reinforced with SiC filaments [33].

Chapter 4

4D Printing

Additive manufacturing is one of the essential processes to create smart structures with shape memory polymers [33]. The 3D printing concept has evolved into 4D printing by using smart materials that can respond to external stimuli in 3D printing technologies [39, 35]. This technique allows the fabrication of dynamically adjustable shapes, properties and functionalities by integrating the dimension of time. It provides shape, functional and material complexity (Figure 4.1).

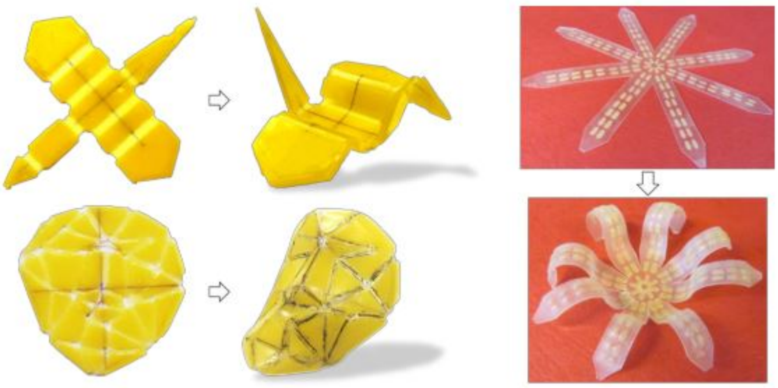

Figure 4.1 Examples of 4D-printed parts [54].

4D printing can solve many real world problems, despite its limitations, such as having to avoid support structures, slow printing times and the lack of low-cost materials [35]. However, shape-shifting behaviour can be reached by printing an entire part in a smart material, as was developed in this dissertation, or by just adding smart hinges in the structure, while having the rest of the part made in conventional materials, therefore decreasing the cost of the piece [35, 34, 53]. On the other hand, using a printing technology means both machining and assembly don't need to be taken into consideration [33].

The potential applications of 4D printed parts can be summarised in [34]:

1. **Self-assembly:** from self-assembling buildings in war zones to space antennae and satellites, this capability is important to create structures in harsh environments with minimum human involvement.

2. **Self-adaptability:** sensing and actuation can be integrated into materials so that external mechanisms aren't necessary, consequently decreasing the number of parts in a certain structure, assembly time, material and energy costs and number of failure-prone devices.

3. **Self-repair:** optimizes reusability and recycling.

All in all, 4D printing can be a huge help in developing smart and complex parts, that allow for structures such as this shelter to be manufactured in one sequence without human intervention and that eliminate the need of posterior assembly and post-processing.

4.1 3D Printing

As previously seen, 4D printing techniques are using a shape memory material in a 3D printing process. 3D printing, also known as additive manufacturing, can be defined as a technology that creates physical objects through successive deposition of material. Currently, there is a vast number of different printing methods, the most common one being fused-deposition modeling (FDM).

FDM is a versatile process that consists of taking a CAD model, extruding plastic filament through a nozzle and depositing it layer-by-layer until the 3D object is formed [55]. Its printers are characterized by its low cost, high reliability and simple operation, as well as safety and efficiency [56, 57, 55].

In this process, as can be observed in Figure 4.2, the filament is first pulled to the nozzle and heated to a semi-liquid state [58]. Then, it is extruded through the nozzle and is deposited on a platform in thin layers. The nozzle is part of the head, which is computer-controlled, as well as the platform. The former moves in the XY plane while the latter moves in the z-direction, according to the g-code written for each specific object. As the material is deposited, it solidifies almost immediately and is bonded to the previous layer [55].

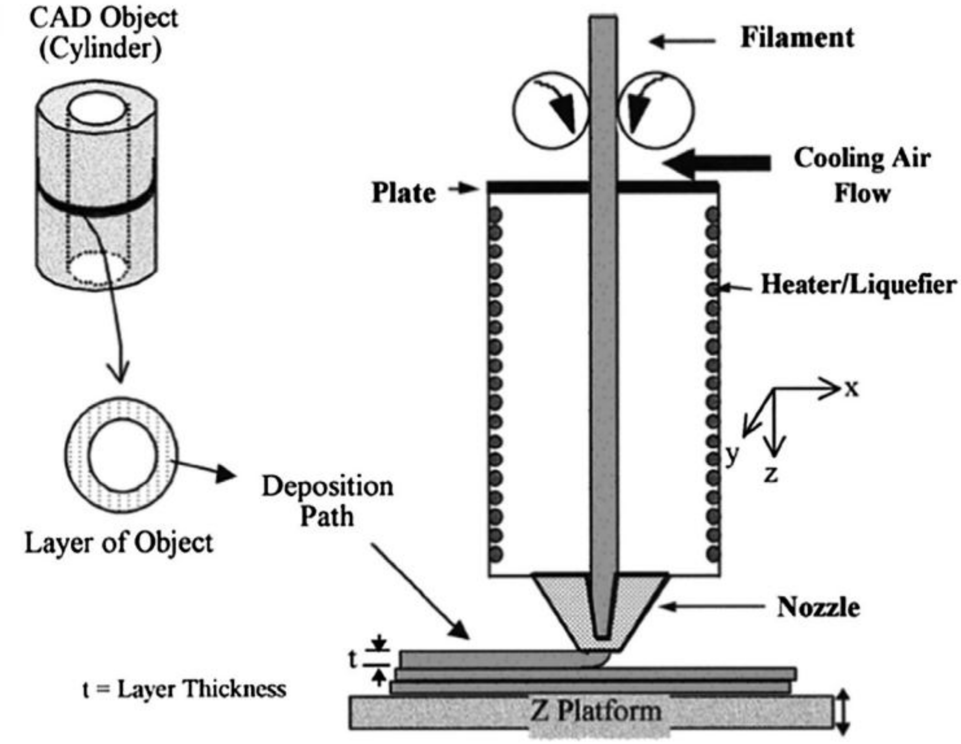

Figure 4.2 Fused-deposition modelling process [58].

This process doesn't use toxic materials, intense heat or laser, machines can be left unattended for hours on end and the printed parts can be handled almost immediately after the process is finished [55]. Using this technology, the quality of the parts is determined not by the operator's skills, but the process and material used. Another clear advantage is that no material is wasted, as opposed to material-removal processes, and before printing a clear prediction of the amount of material and time needed can be accomplished [55, 58].

However, it has some problems when it comes to mass production, since it is a slow process [33]. Accuracy and surface-finish are limited because of the circular geometry of the nozzle and the layer-by-layer deposition, since it can cause a staircase effect and, therefore, a grainy surface. Finally, the final printed parts have different mechanical properties according to each direction [55]. As opposed to the result of a moulding or casting process, in which the part is uniformly consolidated, the printed part is laminated [33]. Consequently, the structure is characterized by having anisotropic properties because of the directional pre-strain and residual stress. This anisotropy can be enhanced by controlling the printing path, which has implications in how the shape transforms. It is also influenced by the infill percentage and layer thickness [51, 57].

When 3D printing, there are three essential parameters to take into consideration since they have an enormous influence on the final part's mechanical properties, accuracy, surface quality and build time [39, 59, 55]:

- **Nozzle temperature** concerns the temperature reached by the filament inside the nozzle and during deposition and it controls the viscosity of the material.

- **Velocity** pertains to the displacement of the nozzle during deposition.

- **Layer height** concerns the displacement of the printing head in the z-axis after the completion of one layer and the initiation of the next one. It affects the build time and the surface quality. The thinner the layer, the longer it takes to print the part but the smoother it is.

4.2 Printing DiAPLEX MM45-20

The previous work on the development of the shelter studied its printing process and optimized the parameters to print the structure in DiAPLEX MM45-20, having in mind the shape memory effect [1].

In that sense, several tests were previously developed for calibration of the parameters in an *Alpha 8* printer [1]. In a sample with a thickness of 1 mm with dimensions less than 100x100x100 mm^3, the shape memory effect was proven. In order to avoid printing support structures, angles were defined to be less than 45°to 55°[1]. It was reached a solution (Figure 4.3), with an hexagonal shape as base and angled walls to improve the folding process, that showed excellent shape memory, since the sample recovered completely its original shape. It should be noted that PTFE sheets were used between the folds to prevent sticking [1].

It was also shown that the shape memory effect can be activated with either immersion of the whole sample in still hot water or simply running hot water [1].

For the purpose of this dissertation, the previously presented study proved to be an excellent starting point. Since a different printer (*Creality CR-10*) was used, only minor adjustments had to be made to the printing parameters (Table 4.1).

Table 4.1 Printing parameters of specimen — *Creality CR-10* printer.

Parameter	
Layer Height	0.24 mm
Infill	100%
Nozzle diameter	0.4 mm
Printing Temperature	210°C
Build Plate Adhesion	40°C
Printing Speed	20 mm/s
Fan Speed	20%

(a) Process of deformation and recovery of a printed sample with 1 mm thickness [1].

(b) Repetition of the process using a PTFE sheet to avoid sticking [1].

Figure 4.3 Process of deformation and recovery with and without protection [1].

Chapter 5

Finite Element Analysis

5.1 Finite Element Method

The Finite Element Method is a numerical method used in real-world problems with complex conditions, in which a domain is divided in several subdomains — called finite elements. The solution to the governing equation is approximated as a linear combination of nodal values and interpolation functions for each one of these elements. Then, the parts are assembled having in consideration the boundary and initial conditions and the solution for the whole domain is obtained [60].

ABAQUS ® software permits the creation, monitoring, diagnostic and visualization of advanced analysis [61]. The elements used in this analysis were 4-node shell elements, commonly called S4 in ABAQUS ®. It is a general-purpose, three-dimensional shell element that provides an accurate solution for both thin and thick shell problems. It is a fully integrated finite-membrane-strain element. The theory behind the Finite Element Method applied to shell elements will be further explained.

Let us consider a global coordinate system x, y and z and a local system x', y' and z' as well as a rectangular shell domain, as can be seen in Figure 5.1.

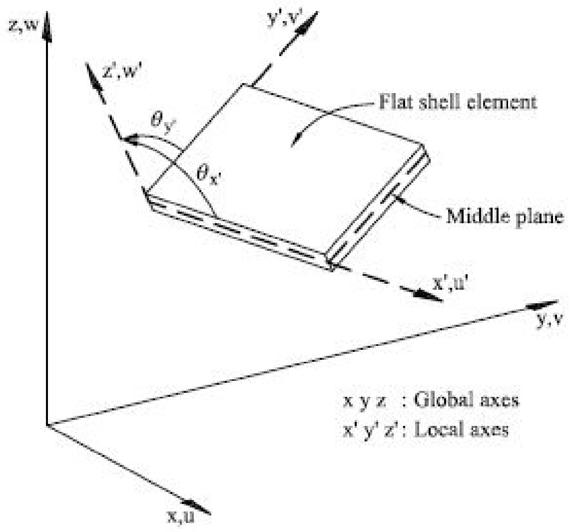

Figure 5.1 Rectangular shell domain [62].

According to Reissler-Mindlin theory, the local displacement vector of a point can be defined as [62]:

$$\boldsymbol{u'} = [u'_0, v'_0, w'_0, \theta_{x'}, \theta_{y'}]^T \tag{5.1}$$

representing three translational displacements and two rotations. A shell structure carries loads in all directions, which means it undergoes bending, twisting and in-plane deformation. The shell element can be formulated by combining the 2D solid element (that handles the in-plane effects — u and v) and the plate element (which handles the bending and off-plane effects — w, θ_x and θ_y) [62, 63].

Assuming plane stress, $\sigma_{z'} = 0$ and, consequently, $\varepsilon_{z'}$ can be excluded from the analysis [64]. Hence, the local strain field can be written as [62]:

$$\boldsymbol{\varepsilon'} = \begin{bmatrix} \varepsilon_{x'} \\ \varepsilon_{y'} \\ \gamma_{x'y'} \\ \gamma_{x'z'} \\ \gamma_{y'z'} \end{bmatrix} = \begin{bmatrix} \frac{\partial u'}{\partial x'} \\ \frac{\partial v'}{\partial y'} \\ \frac{\partial u'}{\partial y'} + \frac{\partial v'}{\partial x'} \\ \frac{\partial u'}{\partial z'} + \frac{\partial w'}{\partial x'} \\ \frac{\partial v'}{\partial z'} + \frac{\partial w'}{\partial y'} \end{bmatrix} = \begin{bmatrix} \frac{\partial u'_0}{\partial x'} \\ \frac{\partial v'_0}{\partial y'} \\ \frac{\partial u'_0}{\partial y'} + \frac{\partial v'_0}{\partial x'} \\ 0 \\ 0 \end{bmatrix} + \begin{bmatrix} -z' \frac{\partial \theta'_x}{\partial x'} \\ -z' \frac{\partial \theta'_y}{\partial y'} \\ -z' \left(\frac{\partial \theta'_x}{\partial y'} + \frac{\partial \theta'_y}{\partial x'} \right) \\ \frac{\partial w'_0}{\partial x'} - \theta_{x'} \\ \frac{\partial w'_0}{\partial y'} - \theta_{y'} \end{bmatrix} \tag{5.2}$$

or [62]:

$$\boldsymbol{\varepsilon'} = \begin{bmatrix} \varepsilon'_{in\mathbf{p}lane} \\ \varepsilon'_{\mathbf{s}hear} \end{bmatrix} = \begin{bmatrix} \varepsilon'_{\mathbf{a}xial} \\ 0 \end{bmatrix} + \begin{bmatrix} -z\varepsilon'_{\mathbf{b}ending} \\ \varepsilon'_{\mathbf{s}hear} \end{bmatrix}. \tag{5.3}$$

In addition, the local stresses are obtained from [62]:

$$\boldsymbol{\sigma'} = \begin{bmatrix} \sigma_{x'} \\ \sigma_{y'} \\ \tau_{x'y'} \\ \tau_{x'z'} \\ \tau_{y'z'} \end{bmatrix} = \begin{bmatrix} \boldsymbol{\sigma'_p} \\ \boldsymbol{\sigma'_s} \end{bmatrix} = \boldsymbol{D'}\boldsymbol{\varepsilon'} + \boldsymbol{\sigma'^0} \tag{5.4}$$

where $\boldsymbol{\sigma'^0}$ represents the initial stress vector and matrix $\boldsymbol{D'}$ for an isotropic material is defined as [62]:

$$\boldsymbol{D'} = \begin{bmatrix} \boldsymbol{D'_p} & 0 \\ 0 & \boldsymbol{D'_s} \end{bmatrix}, \quad \boldsymbol{D'_p} = \frac{E}{1-\nu^2} \begin{bmatrix} 1 & \nu & 0 \\ \nu & 1 & 0 \\ 0 & 0 & \frac{1-\nu}{2} \end{bmatrix}, \quad \boldsymbol{D'_s} = G \begin{bmatrix} 1 & 0 \\ 0 & 1 \end{bmatrix} \tag{5.5}$$

in which G is the Shear Modulus of the material and ν is the Poisson coefficient.

Let V be the shell volume, A the area of the shell surface, $\boldsymbol{t'}$ the surface load vector and $\boldsymbol{p'}$ the concentrated loads and moments, the Principle of Virtual Work is [62]:

$$\iiint_V \delta\boldsymbol{\varepsilon'}^T \boldsymbol{\sigma'} dV = \iint_A \delta\boldsymbol{u'}^T \boldsymbol{t'} dA + \sum_i \delta\boldsymbol{u'_i}^T \boldsymbol{p'_i}. \tag{5.6}$$

From Equations (5.3) and (5.4) and neglecting the initial strains, the previous equation becomes [62]:

$$\begin{aligned}
\iiint_V \delta\boldsymbol{\varepsilon}'^T \boldsymbol{\sigma'} dV &= \iiint_V \delta \left[\boldsymbol{\varepsilon'_a}^T - z'\boldsymbol{\varepsilon'_b}^T, \boldsymbol{\varepsilon'_s}^T\right] \begin{bmatrix} \boldsymbol{\sigma'_p} \\ \boldsymbol{\sigma'_s} \end{bmatrix} dV \\
&= \iiint_V (\delta\boldsymbol{\varepsilon'_a}^T \boldsymbol{\sigma'_p} - z'\delta\boldsymbol{\varepsilon_b}'^T \boldsymbol{\sigma'_p} + \delta\boldsymbol{\varepsilon'_s}^T \boldsymbol{\sigma'_s}) dV, \quad -\frac{t}{2} \leq z' \leq \frac{t}{2} \\
&= \iint_A \left[\delta\boldsymbol{\varepsilon'_a}^T \left(\int_{-\frac{t}{2}}^{+\frac{t}{2}} \boldsymbol{\sigma'_p} dz'\right) + \delta\boldsymbol{\varepsilon'_b}^T \left(\int_{-\frac{t}{2}}^{+\frac{t}{2}} \boldsymbol{\sigma'_p} dz'\right) + \delta\boldsymbol{\varepsilon'_s}^T \left(\int_{-\frac{t}{2}}^{+\frac{t}{2}} \boldsymbol{\sigma'_s} dz'\right)\right] dA \\
&= \iint_A (\delta\boldsymbol{\varepsilon'_a}^T \boldsymbol{\sigma'_a} + \delta\boldsymbol{\varepsilon'_b}^T \boldsymbol{\sigma'_b} + \delta\boldsymbol{\varepsilon'_s}^T \boldsymbol{\sigma'_s}) dA \\
&= \iint_A \delta\boldsymbol{\varepsilon'}^T \boldsymbol{\sigma'} dA
\end{aligned}$$

which means the internal virtual work is the sum of the axial, bending and transversal shear contributions. At last, the integration domain is reduced and the Principle of Virtual Work can be written as

$$\iint_A \delta\boldsymbol{\varepsilon'}^T \boldsymbol{\sigma'} dA = \iint_A \delta\boldsymbol{u'}^T \boldsymbol{t'} dA + \sum_i \delta\boldsymbol{u'}_i^T \boldsymbol{p'}_i. \tag{5.7}$$

Considering the discretization of the shell surface into C^0 isoparametric shell elements with n nodes, being these elements contained in the local plane $x'y'$, the local displacements are interpolated as

$$\boldsymbol{u'} = \sum_{i=1}^{n} \boldsymbol{N_i u'_i} = [N_1, N_2, ..., N_n] \begin{bmatrix} u'_1 \\ u'_2 \\ ... \\ u'_n \end{bmatrix} \tag{5.8}$$

where $\boldsymbol{N_i}$ is the shape function matrix and $\boldsymbol{u_i}$ the local displacement vector of node i (previously presented in Equation (5.1)):

$$\boldsymbol{N_i} = \begin{bmatrix} N_i & 0 & 0 & 0 & 0 \\ 0 & N_i & 0 & 0 & 0 \\ 0 & 0 & N_i & 0 & 0 \\ 0 & 0 & 0 & N_i & 0 \\ 0 & 0 & 0 & 0 & N_i \end{bmatrix}, \quad \boldsymbol{u'_i} = [u'_0, v'_0, w'_0, \theta_{x'}, \theta_{y'}]. \tag{5.9}$$

The shape function for each node can be defined as [65]:

$$N_i = \frac{1}{4}(1 + \xi_i \xi)(1 + \eta_i \eta) \tag{5.10}$$

where ξ and η represent the local coordinates ($-1 \leq \xi, \eta \leq 1$) — see Figure 5.2.

In turn, the discretized strain field is

$$\boldsymbol{\varepsilon} = \begin{bmatrix} \boldsymbol{\varepsilon_m} \\ \boldsymbol{\varepsilon_b} \\ \boldsymbol{\varepsilon_s} \end{bmatrix} = \begin{bmatrix} \frac{\partial u'_0}{\partial x'} \\ \frac{\partial v'_0}{\partial y'} \\ \frac{\partial u'_0}{\partial y'} + \frac{\partial v'_0}{\partial x'} \\ \frac{\partial \theta_{x'}}{\partial x'} \\ \frac{\partial \theta_{y'}}{\partial y'} \\ \frac{\partial \theta_{x'}}{\partial y'} + \frac{\partial \theta_{y'}}{\partial x'} \\ \frac{\partial w'_0}{\partial x'} - \theta_{x'} \\ \frac{\partial w'_0}{\partial y'} - \theta_{y'} \end{bmatrix} = \sum_{i=1}^{n} \begin{bmatrix} \frac{\partial N_i}{\partial x'} u'_{o_i} \\ \frac{\partial N_i}{\partial y'} v'_{0_i} \\ \frac{\partial N_i}{\partial y'} u'_{o_i} + \frac{\partial N'_i}{\partial x'} v'_{o_i} \\ \frac{\partial N_i}{\partial x'} \theta_{x'_i} \\ \frac{\partial N_i}{\partial y'} \theta_{y'_i} \\ \frac{\partial N_i}{\partial y'} \theta_{x'_i} + \frac{\partial N_i}{\partial x'} \theta_{y'_i} \\ \frac{\partial N_i}{\partial x'} w'_{o_i} - N_i \theta_{x'_i} \\ \frac{\partial N_i}{\partial y'} w'_{o_i} - N_i \theta_{y'_i} \end{bmatrix} = \sum_{i=1}^{n} \boldsymbol{B_i u} = [B_1, B_2, ..., B_n] \begin{bmatrix} u'_1 \\ u'_2 \\ ... \\ u'_n \end{bmatrix} = \boldsymbol{Bu} \tag{5.11}$$

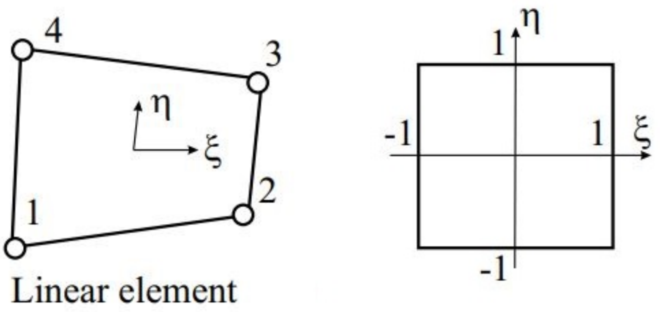

Figure 5.2 Linear finite element and its representation in the local coordinate system [65].

where **B** is the strain matrix defined as

$$\boldsymbol{B_i} = \begin{bmatrix} \boldsymbol{B_a} \\ \boldsymbol{B_b} \\ \boldsymbol{B_s} \end{bmatrix}, \boldsymbol{B_a} = \begin{bmatrix} \frac{\partial N_i}{\partial x} & 0 & 0 & 0 & 0 \\ 0 & \frac{\partial N_i}{\partial y} & 0 & 0 & 0 \\ \frac{\partial N_i}{\partial y} & \frac{\partial N_i}{\partial x} & 0 & 0 & 0 \end{bmatrix}$$

$$\boldsymbol{B_b} = \begin{bmatrix} 0 & 0 & 0 & \frac{\partial N_i}{\partial x} & 0 \\ 0 & 0 & 0 & 0 & \frac{\partial N_i}{\partial y} \\ 0 & 0 & 0 & \frac{\partial N_i}{\partial y} & \frac{\partial N_i}{\partial x} \end{bmatrix}$$

$$\boldsymbol{B_s} = \begin{bmatrix} 0 & 0 & \frac{\partial N_i}{\partial x} & -N_i & 0 \\ 0 & 0 & \frac{\partial N_i}{\partial y} & 0 & -N_i \end{bmatrix}.$$

From Equation (5.7), the Principle of Virtual Work applied to one element is

$$\iint_A \delta\boldsymbol{\varepsilon}'^T \boldsymbol{\sigma'} dA = \iint_A \delta\boldsymbol{u}'^T \boldsymbol{t'} dA + \sum_i \delta\boldsymbol{u}_i'^T \boldsymbol{p'}_i = \iint_A \delta\boldsymbol{u'}^T \boldsymbol{t'} dA + [\delta\boldsymbol{a'}]^T \boldsymbol{q'} \tag{5.12}$$

where the vector $\boldsymbol{q}$ is the equilibrating nodal force vector. Introducing Equation (5.4) into the previous one,

$$\iint_A \delta\boldsymbol{\varepsilon}'^T \boldsymbol{D'}\boldsymbol{\varepsilon'} dA + \iint_A \delta\boldsymbol{\varepsilon'}^T \boldsymbol{\sigma'^o} dA - \iint_A \delta\boldsymbol{u'}^T \boldsymbol{t'} dA = [\delta\boldsymbol{a'}]^T \boldsymbol{q'}. \tag{5.13}$$

Following the standard process with the discretizations previously defined, the elementar equilibrium equations are reached:

$$\boldsymbol{q'} = \boldsymbol{K'^e}\boldsymbol{u'^e} - \boldsymbol{f'^e} \tag{5.14}$$

where $\boldsymbol{K}$ is the stiffness matrix defined as

$$K'^{e}_{ij} = \iint_A \boldsymbol{B'}^T_i \boldsymbol{D'} \boldsymbol{B'}_j dA \tag{5.15}$$

and $\boldsymbol{f}$ is the equivalent nodal force vector for the element in local axes considering only the effect of surface loads and initial stresses:

$$\boldsymbol{f'}^{e}_{i} = \iiint_A \boldsymbol{N_i}^T \boldsymbol{t'} dA - \iint_A \boldsymbol{B'^T_i} \boldsymbol{\sigma'^0} dA. \tag{5.16}$$

As previously stated, the shell element is a combination of the 2D solid and the plate elements. Therefore, the stiffness matrices for these two types of elements will be shown next.

The 2D solid element handles the in-plane effects that correspond to the degrees of freedom of u and v. The stiffness matrix determined from this element is called the membrane stiffness matrix and is given by the combination of sub-matrices with a dimension of 2×2 (u and v) for each node [63]:

$$\boldsymbol{k^{e,m}} = \begin{bmatrix} \boldsymbol{k^m_{11}} & \boldsymbol{k^m_{12}} & \boldsymbol{k^m_{13}} & \boldsymbol{k^m_{14}} \\ \boldsymbol{k^m_{21}} & \boldsymbol{k^m_{22}} & \boldsymbol{k^m_{23}} & \boldsymbol{k^m_{24}} \\ \boldsymbol{k^m_{31}} & \boldsymbol{k^m_{32}} & \boldsymbol{k^m_{33}} & \boldsymbol{k^m_{34}} \\ \boldsymbol{k^m_{41}} & \boldsymbol{k^m_{42}} & \boldsymbol{k^m_{43}} & \boldsymbol{k^m_{44}} \end{bmatrix}. \tag{5.17}$$

On the other hand, the stiffness matrix of a plate element handles the bending effects (bending stiffness matrix), which correspond to the degrees of freedom of w, θ_x and θ_y. Consequently, in this case each sub-matrix has a dimension of 3×3 [63]:

$$\boldsymbol{k^{e,b}} = \begin{bmatrix} \boldsymbol{k^b_{11}} & \boldsymbol{k^b_{12}} & \boldsymbol{k^b_{13}} & \boldsymbol{k^b_{14}} \\ \boldsymbol{k^b_{21}} & \boldsymbol{k^b_{22}} & \boldsymbol{k^b_{23}} & \boldsymbol{k^b_{24}} \\ \boldsymbol{k^b_{31}} & \boldsymbol{k^b_{32}} & \boldsymbol{k^b_{33}} & \boldsymbol{k^b_{34}} \\ \boldsymbol{k^b_{41}} & \boldsymbol{k^b_{42}} & \boldsymbol{k^b_{43}} & \boldsymbol{k^b_{44}} \end{bmatrix}. \tag{5.18}$$

If these two matrices are combined, the stiffness matrix for the shell element in local coordinates is determined [63]:

$$\boldsymbol{k^e} = \begin{bmatrix} \boldsymbol{k_{11}^m} & 0 & 0 & \boldsymbol{k_{12}^m} & 0 & 0 & \boldsymbol{k_{13}^m} & 0 & 0 & \boldsymbol{k_{14}^m} & 0 & 0 \\ 0 & \boldsymbol{k_{11}^b} & 0 & 0 & \boldsymbol{k_{12}^b} & 0 & 0 & \boldsymbol{k_{13}^b} & 0 & 0 & \boldsymbol{k_{14}^b} & 0 \\ 0 & 0 & 0 & 0 & 0 & 0 & 0 & 0 & 0 & 0 & 0 & 0 \\ \boldsymbol{k_{21}^m} & 0 & 0 & \boldsymbol{k_{22}^m} & 0 & 0 & \boldsymbol{k_{23}^m} & 0 & 0 & \boldsymbol{k_{24}^m} & 0 & 0 \\ 0 & \boldsymbol{k_{21}^b} & 0 & 0 & \boldsymbol{k_{22}^b} & 0 & 0 & \boldsymbol{k_{23}^b} & 0 & 0 & \boldsymbol{k_{24}^b} & 0 \\ 0 & 0 & 0 & 0 & 0 & 0 & 0 & 0 & 0 & 0 & 0 & 0 \\ \boldsymbol{k_{31}^m} & 0 & 0 & \boldsymbol{k_{32}^m} & 0 & 0 & \boldsymbol{k_{33}^m} & 0 & 0 & \boldsymbol{k_{34}^m} & 0 & 0 \\ 0 & \boldsymbol{k_{31}^b} & 0 & 0 & \boldsymbol{k_{32}^b} & 0 & 0 & \boldsymbol{k_{33}^b} & 0 & 0 & \boldsymbol{k_{34}^b} & 0 \\ 0 & 0 & 0 & 0 & 0 & 0 & 0 & 0 & 0 & 0 & 0 & 0 \\ \boldsymbol{k_{41}^m} & 0 & 0 & \boldsymbol{k_{42}^m} & 0 & 0 & \boldsymbol{k_{43}^m} & 0 & 0 & \boldsymbol{k_{44}^m} & 0 & 0 \\ 0 & \boldsymbol{k_{41}^b} & 0 & 0 & \boldsymbol{k_{42}^b} & 0 & 0 & \boldsymbol{k_{43}^b} & 0 & 0 & \boldsymbol{k_{44}^b} & 0 \\ 0 & 0 & 0 & 0 & 0 & 0 & 0 & 0 & 0 & 0 & 0 & 0 \end{bmatrix}. \tag{5.19}$$

In the local coordinate system, there is no θ_z; accordingly, the components related to this degree of freedom are null.

In the global coordinate system, at a node of a shell element there are six degrees of freedom (DOF): three translational displacements and three rotations. For a rectangular shell element (4 nodes), the displacement vector can be defined as [63]:

$$\boldsymbol{a^e} = \begin{bmatrix} \boldsymbol{a_1} \\ \boldsymbol{a_2} \\ \boldsymbol{a_3} \\ \boldsymbol{a_4} \end{bmatrix} \tag{5.20}$$

in which $\boldsymbol{a_i}(i = 1, 2, 3, 4)$ represent the displacement vector at node i [63]:

$$\boldsymbol{a_i} = \begin{bmatrix} u_i \\ v_i \\ w_i \\ \theta_{xi} \\ \theta_{yi} \\ \theta_{zi} \end{bmatrix}. \tag{5.21}$$

Transforming the matrices from Equations (5.19) to the global coordinate system [63],

$$\boldsymbol{K^e} = \boldsymbol{T}^T \boldsymbol{k^e} \boldsymbol{T} \tag{5.22}$$

$$\boldsymbol{F}^e = \boldsymbol{T}^T \boldsymbol{f}^e \tag{5.23}$$

with

$$\boldsymbol{T} = \begin{bmatrix} \boldsymbol{T_3} & 0 & 0 & 0 & 0 & 0 & 0 & 0 \\ 0 & \boldsymbol{T_3} & 0 & 0 & 0 & 0 & 0 & 0 \\ 0 & 0 & \boldsymbol{T_3} & 0 & 0 & 0 & 0 & 0 \\ 0 & 0 & 0 & \boldsymbol{T_3} & 0 & 0 & 0 & 0 \\ 0 & 0 & 0 & 0 & \boldsymbol{T_3} & 0 & 0 & 0 \\ 0 & 0 & 0 & 0 & 0 & \boldsymbol{T_3} & 0 & 0 \\ 0 & 0 & 0 & 0 & 0 & 0 & \boldsymbol{T_3} & 0 \\ 0 & 0 & 0 & 0 & 0 & 0 & 0 & \boldsymbol{T_3} \end{bmatrix} \tag{5.24}$$

and

$$\boldsymbol{T_3} = \begin{bmatrix} l_x & m_x & n_x \\ l_y & m_y & n_y \\ l_z & m_z & n_z \end{bmatrix} \tag{5.25}$$

where l, m and n are the direction cosines.

Substituting in Equation (5.28), it finally gives the equilibrium equation for the element in global coordinate system:

$$\boldsymbol{q}^e = \boldsymbol{K}^e \boldsymbol{a}^e - \boldsymbol{f}^e. \tag{5.26}$$

5.2 Sensitivity Analysis

A Design Sensitivity Analysis (DSA) can be performed using ABAQUS ® capabilities, providing the sensitivities of responses with respect to certain design parameters. These parameters range from material and/or section properties, concentrated forces and moments, and nodal coordinates. This study is helpful in parameter importance analysis and, consequently, design optimization, since it shows the influence ratio of a certain structural response with respect to a perturbation of another variable [66].

Mathematically, sensitivities are the derivatives of specified variables (design responses) with respect to chosen design parameters, as they provide a first-order measure of how sensitive the variables are to a change in the design parameters. They are obtained using both the direct differentiation method (DDM), the semi-analytical computational technique and, by default, the central differencing scheme [61]. As opposed to the finite difference method, the DDM provides an exact value for the sensitivity with minimal computational cost [67]. It involves deriving analytical expressions for the response gradients, directly differentiating the finite element equations, without having to perform additional simulations for each parameter [66, 67].

The equations can be derived based on a total displacement formulation for history-independent problems, where the current state of the problem depends only on the total displacement. Basically, the sensitivities do not depend on sensitivity results calculated in previous increments.

Let A and B be the numbers of responses and parameters and each response ϕ_a $(a = 1, ..., A)$ be a function of parameters $(b = 1, ..., B)$ depending on them both explicitly and via the displacement filed represented by the nodal displacement vector u (the dependence $u(h_b)$ is implicit) [61]:

$$\phi_a = \phi_a(u(h_b), h_b). \tag{5.27}$$

The equilibrium problem is defined by [61]:

$$\int_V \beta\tau dV = \int_S N^T t dS + \int_V N^T f dV. \tag{5.28}$$

Assuming that this problem has been solved at the end of an increment and that the converged solution u and the values of all responses are known, the sensitivity of a response ϕ_a with respect to a design parameter h_b can be defined as [61]:

$$\frac{d\phi_a}{dh_b} = \frac{\partial\phi_a}{\partial h_b} + \frac{\partial\phi_a}{\partial u}\frac{du}{dh_b}. \tag{5.29}$$

There is only one unknown quantity in the previous equation: $\frac{du}{dh_b}$. Consequently, in order to compute it, a system of equations needs to be solved. Equation (5.28) can be rewritten as [61]:

$$F(u) = 0 = -\int_{V^0} \beta\tau dV^0 + \int_S N^T t dS + \int_V N^T f dV. \tag{5.30}$$

Next, differentiation with respect to design parameters gives [61]:

$$K\frac{du}{dh_b} = -\frac{\partial F}{\partial h_b} \tag{5.31}$$

where $K = \frac{\partial F}{\partial u}$ is the Jacobian matrix and $\frac{\partial F}{\partial h_b}$ is a determinable quantity. Substituting in Equation (5.29), the solution of the total displacement DSA problem is reached [61]:

$$\frac{d\phi_a}{dh_p} = \frac{\partial \phi_a}{\partial h_p} - \frac{\partial \phi_a}{\partial u} K^{-1} \frac{\partial F}{\partial h_b}. \tag{5.32}$$

The algorithm used is the direct differentiation method. After obtaining the converged solution, $\frac{\partial \phi_a}{\partial h_b}$, $\frac{\partial \phi_a}{\partial u}$ and $\frac{\partial F}{\partial h_b}$ have to be computed element-by-element. The final solution is determined by solving Equation (5.31) for each $b = 1, ...B$ with respect to the unknown vectors of nodal displacement sensitivity, which are then substituted in Equation (5.29) to calculate $\frac{d\phi_a}{dh_b}$ [61].

Chapter 6

Structural Design

In this chapter, the loads applied to the shelter are calculated, using the EN Eurocode to determine the overload, self weight, wind and snow loads. Afterwards, the possible combinations of these loads are composed. Finally, the design and structural requirements are presented. It should be noted that the situation studied represents a very extreme one.

As previously stated, in order to analyse the shelter structurally, the EN Eurocode was followed. This is a group of ten standards regarding subjects involved with construction and structural design — see Figure 6.1. Each standard covers technical aspects such as actions on structures, design of buildings for fire, design of bridges and design of concrete, steel and other materials, among others [68]. For the purpose of this dissertation, *EN 1990 (Basis of structural design)* and *EN 1991 (Actions on structures)* were applied.

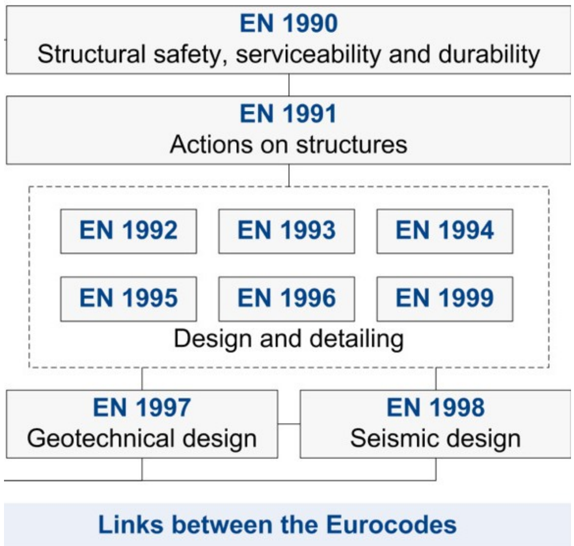

Figure 6.1 Links between Eurocode parts [68].

6.1 Overload

Since the structure is self deployed, it is not predictable that the cover will have to be accessed and since it is a short-duration shelter it is also not foreseeable to have any equipment on the cover. However, it is known that displaced people often need to improve or repair their shelter which means that option was taken into account. Therefore, a cover of Category H (non-accessible covers, except for maintenance and fixing operations) was considered, which gives the uniformly distributed q_k and the concentrated overload Q_k [69]:

$$q_k = 0.4\,\mathrm{kN/m^2}$$
$$Q_k = 1.0\,\mathrm{kN}$$

The overload also covers the possibility of raining.

6.2 Self Weight

The self weight was calculated automatically by ABAQUS ® as a *Gravity* load, by introducing in the software the density of the material and the value of gravity force.

6.3 Wind

According to *Eurocode 1: Actions on structures — Part 1-4: General Actions — Wind Loads (EN 1991-1-4:2005)*, the wind loads applied to the shelter are determined. First, the characteristic value of the peak dynamic pressure (q_p) is calculated, then the pressure coefficients and finally, by multiplying these factors, the final wind pressure on the walls of the shelter (w) is determined.

The peak dynamic pressure q_p is given by [69]:

$$q_p = [1 + 7\,I_v(z)]\,\frac{1}{2}\,\rho\,v_m^2(z) \tag{6.1}$$

where I_v is the air turbulence, ρ is the air density and v_m is the wind's average speed [69].

In turn, air turbulence I_v is given by [69]:

$$I_v(z) = \begin{cases} \dfrac{k_I}{c_o(z)\,ln(z/z_0)}, & \text{if } z_{min} \leq z \leq z_{max} \\ I_v(z_{min}), & \text{if } z < z_{min} \end{cases} \tag{6.2}$$

where k_I is the turbulence coefficient (with a recommended value of 1.0), c_o is the orography coefficient (also 1.0), z is the shelter's height (equal to 2.6 m), z_0 is the roughness length and z_{min} and z_{max} are the minimum and maximum heights [69]. The value of the roughness length z_0 and minimum height z_{min} depend on the type of land, according to Table 6.1. Here, the worst case scenario is considered, which is land of type 0. This results in $z_0 = 0.003\,\text{m}$ and $z_{min} = 1\,\text{m}$ [69].

Table 6.1 Values of z_0 and z_{min} for different types of land [69].

Type	**Description**	z_0 [m]	z_{min} [m]
0	Sea or exposed to sea winds	0.003	1
I	Lakes or flat area with no obstacles/vegetation	0.01	1
II	Area with small vegetation and obstacles separated at a distance >20 times their height	0.05	2
III	Area with obstacles separated at a distance <20 times their height	0.3	5
IV	Area in which at least 15% of surface has building with height >15 m	1.0	1.0

Finally, the value of z_{max} is defined in the standard as 200 metres [69]. Invoking Equation (6.2), and since z is between z_{min} and z_{max},

$$I_v(2.6\,\text{m}) = \frac{1.0}{1.0 \times ln(2.6/0.003)} = 0.14783.$$

The value of ρ depends on the altitude, temperature and atmospheric pressure in the region considered. However, and since those factors are unknown, it is considered the recommended value, which is $1.25\,\text{kg/m}^3$ [69]. Lastly, the average speed v_m was considered 160 km/h (44 m/s). Therefore, according to Equation (6.1), the peak dynamic pressure is

$$q_p = [1 + 7 \times 0.14783] \times \frac{1}{2} \times 1.25 \times 44^2 = 2462.12\,\text{N/m}^2.$$

In order to determine the pressure coefficients, the shelter was considered to be a circular dome with three main zones: A, B and C — see Figure 6.2.

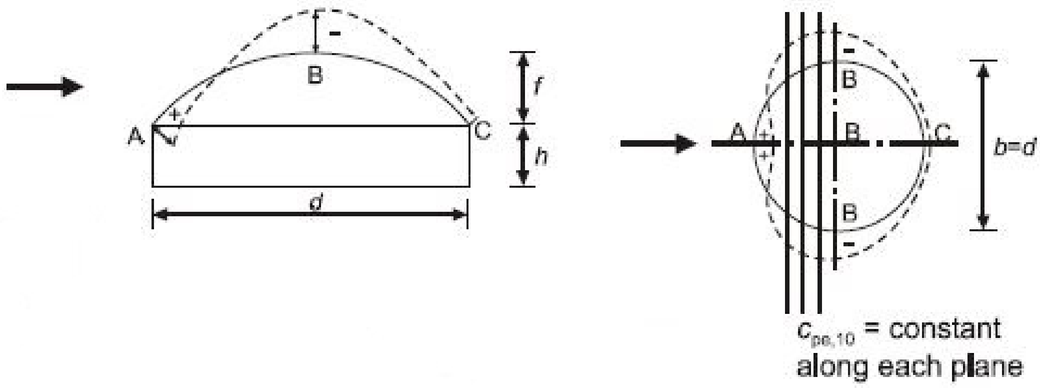

Figure 6.2 Representation of zones of a dome [69].

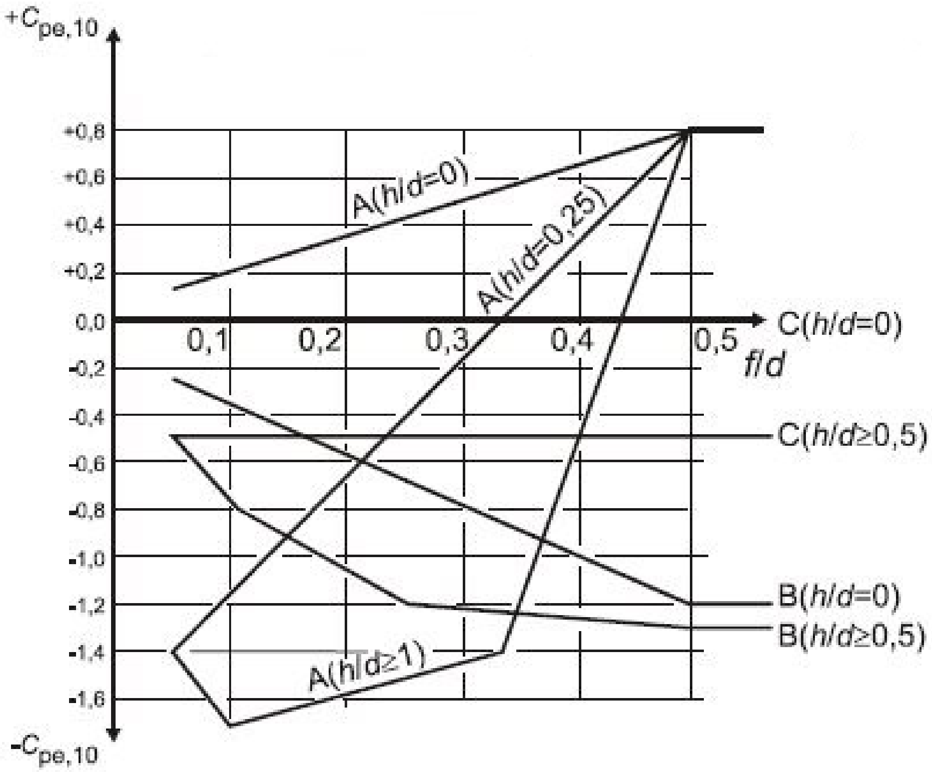

Figure 6.3 Value of pressure coefficients of zones A, B and C of a dome [69].

Considering that $f = 1.6\,\mathrm{m}$, $h = 1\,\mathrm{m}$ and $d = 3.5\,\mathrm{m}$, then f/d is 0.46 and $h/d = 0.29$. By interpolation of the values represented on the graph of Figure 6.3, the exterior pressure coefficients, which are constant along each plane can be determined as [69]:

$$c_{pe}(A) = +0.7$$
$$c_{pe}(B) = -1.2$$
$$c_{pe}(C) = -0.3$$

Simultaneously, there is also interior pressure, which depends on the number and dimension of openings [69]. In this case, it is considered to only exist one opening, the door, and it is also considered that it is usually closed. Therefore, there are no predominant faces and the value of the interior pressure coefficients must be the worst between $+0.2$ and -0.3 [69]. Following, the values of final pressure coefficients are calculated and can be seen in Table 6.2. Comparing the results obtained, both situations need to be further evaluated since it is not possible to deduce immediately which is the worst situation.

Table 6.2 Values of $c_{p,final}$ for each zone of the dome — transverse direction

Zone	**With** $c_{pi} = +0.2$	**With** $c_{pi} = -0.3$
A	+0.5	+1.0
B	-1.4	-0.9
C	-0.5	0.0

Lastly, the final wind pressure can be calculated by multiplying the peak dynamic pressure ($q_p = 2462.096\,\mathrm{N/m^2}$) by the situations shown in Table 6.3:

Table 6.3 Values of w_{final} for each zone of the dome [kN/m^2] — transverse direction.

Zone	**Wind 3** (with $c_{pi} = +0.2$)	**Wind 4** (with $c_{pi} = -0.3$)
A	1.231	2.462
B	-3.447	-2.216
C	-1.231	0.000

The wind with a longitudinal direction also needs to be taken into consideration.

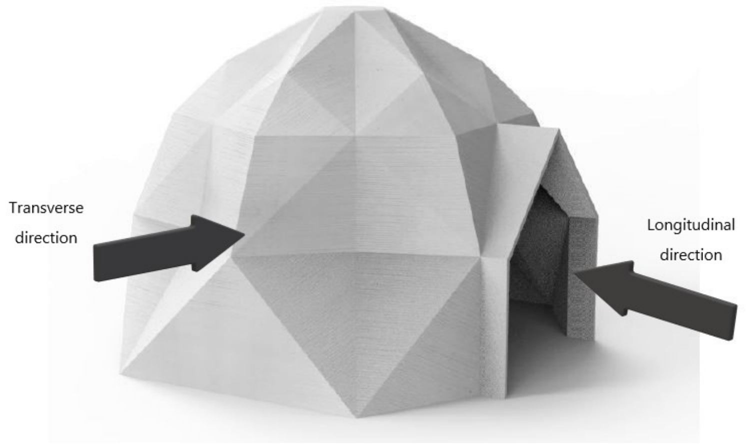

Figure 6.4 Directions of wind — transverse and longitudinal to shelter.

Similarly, two additional situations were determined.

$$c_{pe}(A) = +0.5$$
$$c_{pe}(B) = -1.1$$
$$c_{pe}(C) = -0.3$$

Table 6.4 Values of $c_{p,final}$ for each zone of the dome — longitudinal direction.

Zone	**With** $c_{pi} = +0.2$	**With** $c_{pi} = -0.3$
A	+0.3	+0.8
B	-1.3	-0.8
C	-0.5	0.0

Table 6.5 Values of w_{final} for each zone of the dome [kN/m^2] — longitudinal direction.

Zone	**Wind 1** (with $c_{pi} = +0.2$)	**Wind 2** (with $c_{pi} = -0.3$)
A	0.7386	1.9697
B	-3.2007	-1.9697
C	-1.2311	0.000

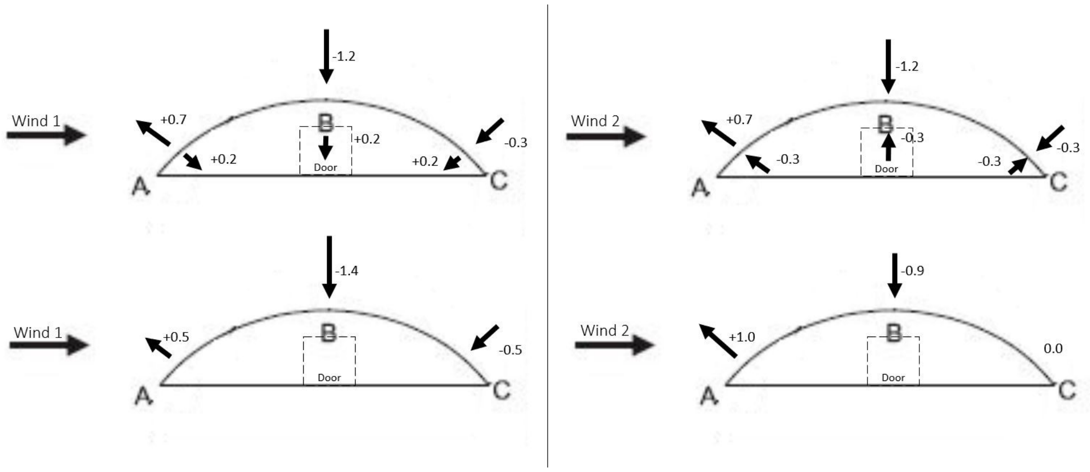

Figure 6.5 Scheme with values of c_{pi} and c_{pe} on top and values of $c_{p,final}$ on the bottom — transverse wind.

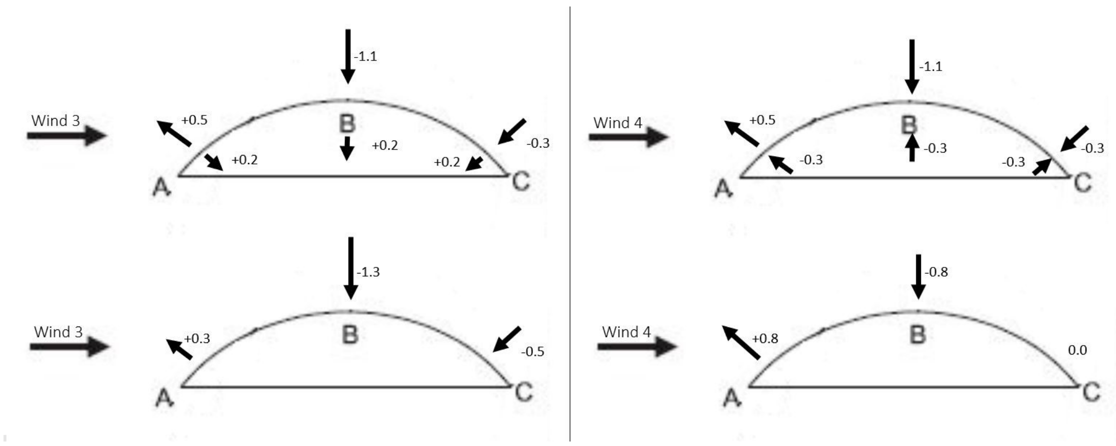

Figure 6.6 Scheme with values of c_{pi} and c_{pe} on top and values of $c_{p,final}$ on the bottom — longitudinal wind.

6.4 Snow

According to *Eurocode 1: Actions on structures — Part 1-3: General Actions — Snow Loads (EN 1991-1-3:2003)*, the snow load was calculated for the worst case scenario.

Generally, the snow load s is calculated by [69]:

$$s = \mu_i \, C_e \, C_t \, s_k \tag{6.3}$$

where μ_i is the shape coefficient for the snow load, C_e is the exposure coefficient, C_t is the thermal coefficient and s_k is the snow load characteristic value.

The shape coefficient for the snow load is related to the shape of the cover. Due to the geometrical cases represented in the standard, a cylindrical cover such as the one represented in Figure 6.7 was considered.

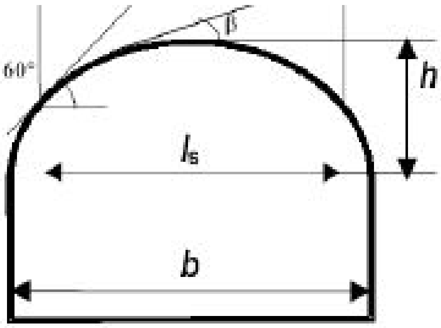

Figure 6.7 Cylindrical cover [69].

The shape coefficient is given by [69]:

$$\mu = 0.2 + 10\,h/b = 4.2$$

where h and b are represented in Figure 6.7 and are equal to 1600 mm and 4000 mm, respectively. However, a maximum value of 2.0 is given for μ [69].

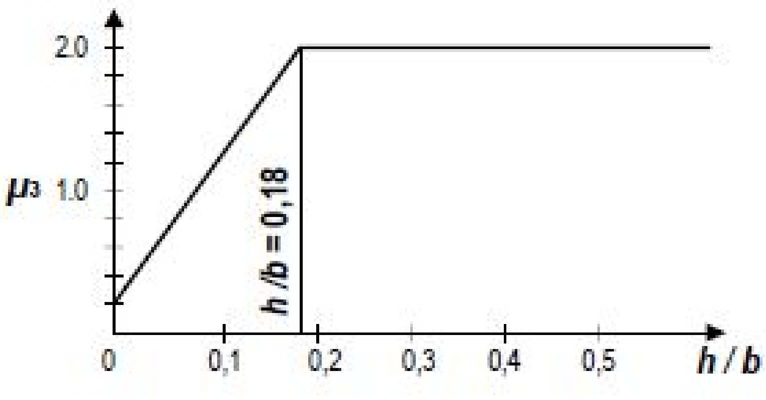

Figure 6.8 Evolution of μ for a structure with a cylindrical cover [69].

Is it stated that C_e should be considered as unitary, unless there is a very specific topography relative to wind exposure — see Table 6.6 [69]. Since in this case the wind exposure is probably normal or high, a value of 1 will be considered.

Table 6.6 Exposure coefficient for different topographies [69].

Topography	C_e
Exposed to wind	0.8
Normal	1.0
Protected from wind	1.2

The thermal coefficient must be also be unitary, unless the cover of the structure has high thermal transmission ($> 1\text{W/m}^2$) [69].

The value of s_k was defined considering the worst case scenario in Europe: Norway. The map represented in Figure 6.9 shows the value of s_k by region in Norway. Therefore, $s_k = 9.5\,\text{kN/m}^2$ [69].

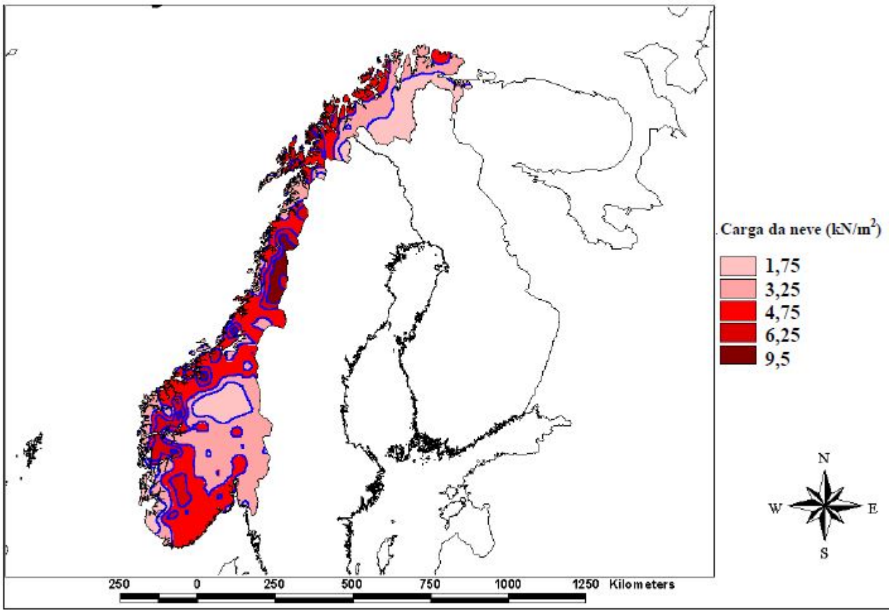

Figure 6.9 Snow load characteristic values in Norway [69].

Finally, using Equation (6.3), the snow load s can be calculated as

$$s = 2.0 \times 1.0 \times 1.0 \times 9.5 = 19\,\text{kN/m}^2.$$

6.5 Combinations

Different combinations of the previous loads result in different responses of the shelter. Therefore, the worst situations need to be analysed with regard to the ultimate limit state. In this case, it is important to assure that the structure does not break or deform excessively because it will stop serving its function. For this reason, the ultimate limit state STR was verified [69].

Generally, combinations of actions are shown in Table 6.7 and they consist of one permanent action (PA), one base variable action (BVA) and one or more accompanying variable actions (AVA). There is only one permanent action, which is self weight [69].

Table 6.7 Combinations.

Combination	**PA (G)**	**BVA ($Q_{k,1}$)**	**AVA 1**	**AVA 2**
1	Self Weight	Overload	-	-
2	Self Weight	Overload	Snow	-
3	Self Weight	Overload	Snow	Wind
4	Self Weight	Overload	Wind	-
5	Self Weight	Snow	-	-
6	Self Weight	Snow	Wind	-
7	Self Weight	Wind	-	-
8	Self Weight	Wind	Snow	-

As it was shown before, there are various situations of snow and wind that need to be considered. These combinations of actions can be expressed as [1] [69]:

$$\gamma_G\, G \quad \text{"}+\text{"} \quad \gamma_{Q,1}\, Q_{k,1} \quad \text{"}+\text{"} \quad \sum_{i>1} \gamma_{Q,i}\, \phi_{0,i}\, Q_{k,i}. \tag{6.4}$$

The coefficient γ for the BVA must be 1.50 and the one for the AVA is also 1.50 in unfavourable cases and 0.0 in favourable ones (always in relation to the BVA). Here, it is always considered 1.50.

For Norway and places situated higher than 1000 metres, the coefficient ϕ_0 for the snow loads is equal to 0.70, and for other places, ϕ_0=0.50. For the overload $\phi = 0$ (this is the reason why AVA are never overload) and for the wind load $\phi_0 = 0.6$ [69].

After including the different types of snow and wind and considering the coefficients for each load, it is possible to summarize the analysed combinations in Table 6.8.

[1]The symbol " + " means *in combination with*.

Table 6.8 Analysed combinations.

Combination	Coef.	PA	Coef.	BVA	Coef.	AVA
1	1.35	Self Weight	1.5	Snow	1.5×0.6	Wind 1
2						Wind 2
3						Wind 3
4						Wind 4
5			1.5	Wind 1	1.5×0.7	Snow
6				Wind 2		
7				Wind 3		
8				Wind 4		
9			1.5	Overload	—	—
10					1.5×0.6	Wind 1
11						Wind 2
12						Wind 3
13						Wind 4
14					1.5×0.7	Snow

6.6 Structural requirements

According to the *EUROCOMP Design Code and Handbook*, which is mainly concerned with glass fibre reinforced thermosetting polymer composites, the maximum deflection for general applications is L/175, in which L is the span [70]. Since the plates that compose the shelter vary in size, the maximum deflection also varies. However, the maximum displacements acceptable in the simulations are always in the same area of the shelter, in which the maximum calculated deflection is 4.86 mm. The *EN Eurocode* for metallic structures establishes a similar, but even more limiting requirement. However, it should be noted that both metals and thermosetting polymers are less deformable than thermoplastic polymers which means a displacement higher than 4.86 mm should not exclude a solution.

The total mass of the shelter is not a structural or design requirement, but a transportation one. If shelters are to be transported on pallets by boat or airplane, their weight should be kept to a minimum, for numerous reasons: not only the cost of transportation will be lower if more units can be transported at once, but also each unit will be easier to handle by the workers or even the displaced people who will need to manipulate them. In Chapter 2, it was seen that the UNHCR tents weigh around 80 kg.

Chapter 7

Numerical Approach

This chapter shows the results of the simulations performed in ABAQUS ®, having in consideration all the iterations made to the shelter.

Firstly, the shelter was analysed as it was previously presented in [1]. Then, pillars were added, followed by a solution involving a reinforcement skeleton with support bars. Lastly, a sandwich structure material was studied with the goal of achieving more rigidity and less mass.

7.1 Static Analysis

7.1.1 Initial shelter

The simulation was prepared using shell sections as well as 4-node shell elements (S4: A 4-node doubly curved thin or thick shell, full-integration, finite membrane strains). Several values of thickness were studied, having in mind that, in terms of weight, a thickness of 1.5 mm was ideally determined in the previous work.

The material used was the DiAPLEX MM45-20 and it was considered to be isotropic (see Table 7.1). A simplification was made here, since the printed material is anisotropic, however it would be very difficult to assume non-isotropy since this material, as was previously seen, is not very much studied and therefore not much information about its properties is available in literature.

At this point, all combination of loads were introduced on the analysis to be studied (Self weight as a *Gravity* load, Wind as *Pressure* and both Snow and Overload as *Surface Traction* loads). The only boundary condition added was fixing the base of the shelter (Figure 7.1). Practically, the way to achieve this could be by putting bags of sand on the bottom rim. Then, a Static Analysis was performed.

Table 7.1 Properties of the material for the simulation performed in ABAQUS ®.

Elastic Modulus	2000 MPa
Poisson Coefficient	0.49
Density	1200 kg/m^3

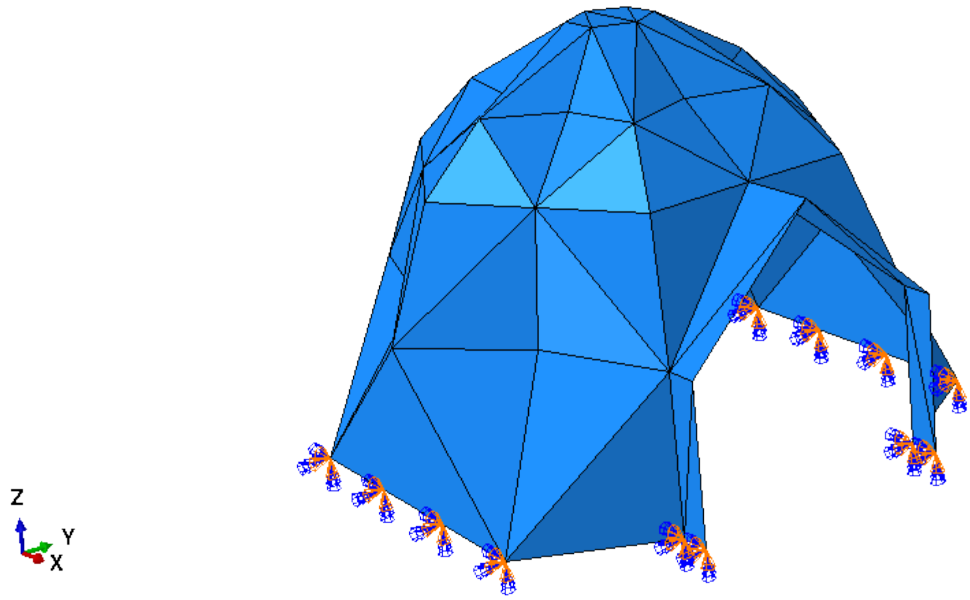

Figure 7.1 Boundary conditions introduced on the shelter.

With the conditions previously mentioned and at the worst load case, the results of the static analysis give a maximum displacement of almost 60 metres. When the thickness is increased the values of displacement decrease but the final mass becomes too high (Table 7.2).

Table 7.2 Variation of shell thickness — DiAPLEX MM45-20.

Section thickness (mm)	**Maximum displacement** (mm)	**Mass** (kg)
1.5	59210	50.4
3	7590	101
4.5	2318	151
6	1011	201
10	240.2	336
15	80.55	504

A solution with reinforced material was considered to improve the results, using glass fiber. Specifically, first using a fiberglass mat which results theoretically in an Elastic Modulus of 8 GPa and a density of 1700 kg/m^3 with 30% of reinforcement. This was still not enough to obtain good results, which meant another solution was considered using glass fiber, resulting in 20 GPa and 1900 kg/m^3 of density. Table 7.3 shows the results for simulations using reinforced material.

Table 7.3 Variation of shell thickness — reinforced material.

Section Thickness (mm)	**Maximum displacement** (mm)		**Mass** (kg)	
	8 GPa	**20 GPa**	**8 GPa**	**20 GPa**
1.5	14800	5921	71.5	79.9
3	1898	759	143	160
4.5	579.5	231.8	215	240
6	252.7	101.1	286	320
10	60.06	24.02	477	533
15	20.14	8.055	715	799

Figure 7.2 shows the displacement results for the shelter with 1.5 mm of thickness and reinforced SMP with 8 GPa of modulus. This figure shows a pattern: the biggest displacements constantly appear in the area of the door. It should be noted that the representation is exaggerated as its only purpose is to accomplish the previous conclusion about critical areas to be improved.

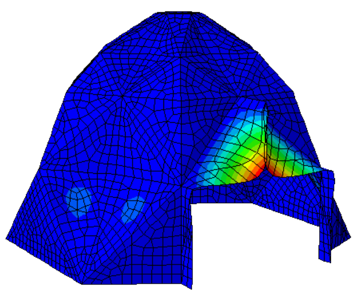

Figure 7.2 Results of displacement to show critical area.

7.1.2 Shelter with pillars

By analysing the previous results, it became clear that the door area is very fragile and the worst results are obtained there. Therefore, pillars were added to support the door (Figure 7.3).

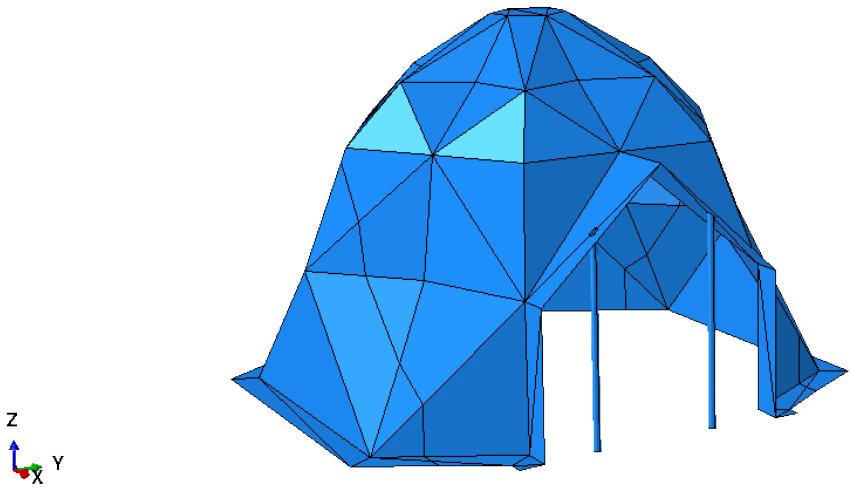

Figure 7.3 Pillars and rim introduced on the shelter.

This solution was studied with pillars made of two materials: the same SMP as the rest of the shelter and steel. The pillars were considered fixed to the ground — see Figure 7.3.

It can be concluded that the difference between the results is not significant (Figure 7.4 shows the curve of results for the simulation with steel and SMP pillars; the graph shows that the pairs of curves for the same SMP are almost overlapped) and, therefore, it is preferable to use the same material because that way only one manufacturing process is used. A similar work was developed for the dimension of the pillars and the conclusion is that it does not influence the displacement values significantly. The final results for SMP pillars are shown in Table 7.4.

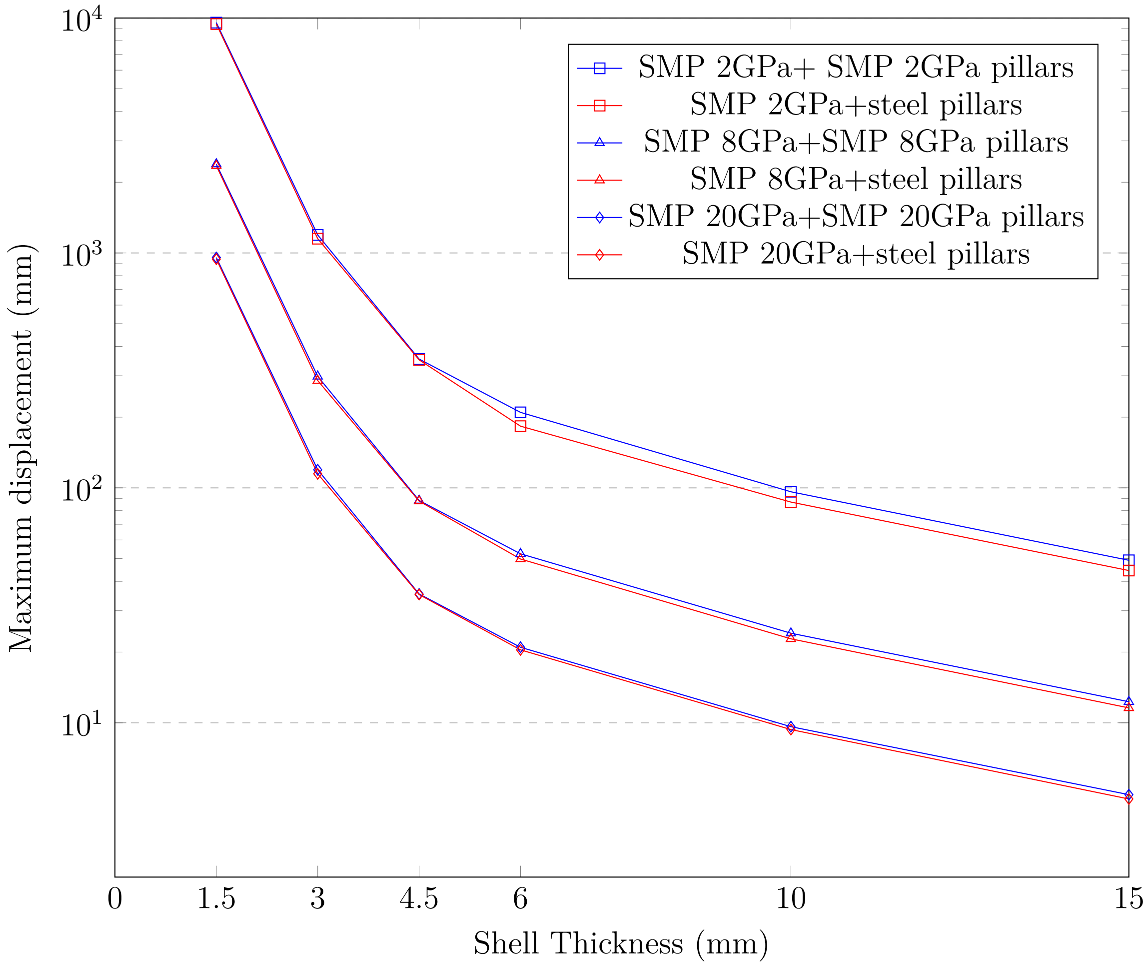

Figure 7.4 Variation of SMP and pillars.

Table 7.4 Variation of shell thickness — SMP pillars.

Section thickness (mm)	**Maximum displacement** (mm)		
	2 GPa	8 GPa	20 GPa
1.5	9560	2390	956
3	1193	298.3	119.4
4.5	353.5	88.38	35.35
6	209.6	52.4	20.96
10	96.24	24.06	9.624
15	49.17	12.29	4.493

The addition of pillars improved the results in the door substantially. Consequently, this modification was maintained in the following iterations.

7.1.3 Shelter with pillars and reinforcement bars

As previously seen, the solution of adding pillars to the structure improves the results in the door. However, the maximum displacement is still much higher than the requirement. Therefore, a solution to add additional bars along the edges of the plates, as a skeleton, was studied (Figure 7.5).

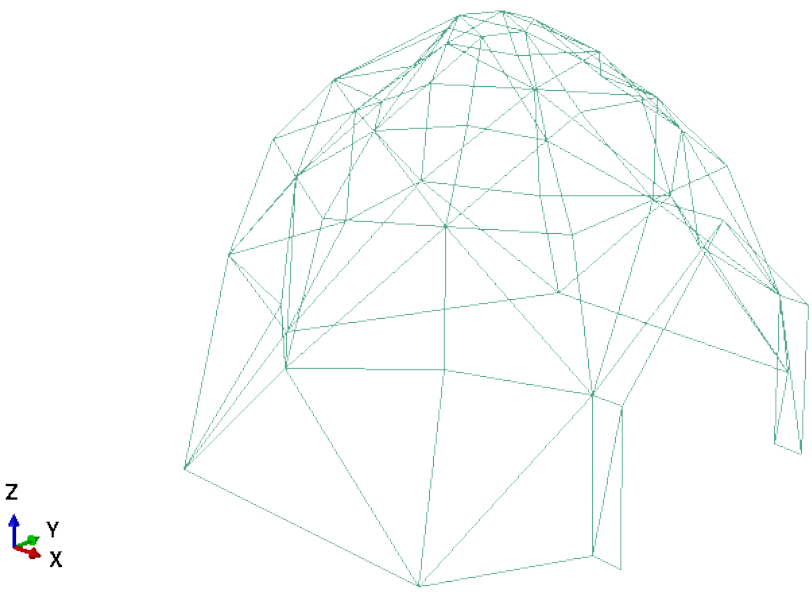

Figure 7.5 Reinforcement bars introduced on the shelter.

Firstly, bars ($d = 15\,\mathrm{mm}$ and $t = 3\,\mathrm{mm}$; a quadrangular profile was considered but adds more weight to the structure than circular profiles without a better performance) were added only along the edges and the result is presented on Table 7.5. This skeleton adds more than 20 kg to the structure (depending on the reinforced material used).

Table 7.5 Variation of shell thickness — with bars along the edges.

Section thickness (mm)	**Maximum displacement (mm)**		
	2 GPa	8 GPa	20 GPa
1.5	9440	2356	942.4
3	1150	288.8	115.5
4.5	369.9	89.43	35.77

In the attempt of coming up with a solution without the need of reinforcing the SMP, an alteration was made and more bars were added, with the goal of supporting the middle of the plates. Results improved, however better results were accomplished without these bars because of the extra weight of the skeleton. Bearing this in mind, this solution was abandoned.

7.1.4 Shelter with sandwich structure

In order to improve the rigidity of the shelter and, at the same time, minimize the weight's growth, a new solution was studied: developing a sandwich structure made out of two thin SMP sheets at the extremities with a core.

Having the work of a FEUP investigator in mind, five geometries for the core were analysed [71] — see Figure 7.6.

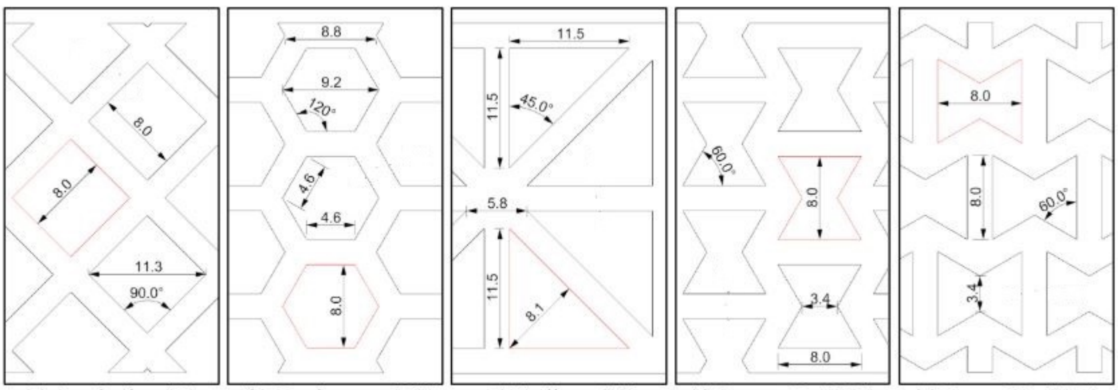

(a) Quadrado - [Q] (b) Hexágono – [H] (c) Treliça – [T] (d) Reent. V – [RV] (e) Reent. H – [RH]

Figure 7.6 Geometry of the cores studied in previous work [71].

According to his studies, which consisted of printing specimens and testing them, core T is the most rigid, but it shows an abrupt rupture with a low displacement.

Core Q, on the other hand, is much more flexible and lighter but doesn't support the same high loads. Cores RH and RV give the worst result when it comes to rigidity and similar masses [71]. Consequently, a solution using cores RH and RV wasn't taken into consideration.

Before modelling the sandwich structure to the whole shelter, a comparison between three possible structures (core Q, H and T with the dimensions presented on Figure 7.6, height of core of 5 mm and thickness of outside sheets of 0.5 mm) was performed by modelling a rectangular plate, supported on both extremities and with two loads applied: self-weight and a surface pressure. Both maximum displacement and mass were determined by doing a static analysis on ABAQUS ® (the absolute values of the results have no physical meaning, it's the comparison which is of interest) — see Table 7.6.

Table 7.6 Variation of type of core on a rectangular plate.

Core	**Max. displacement** (mm)	**Mass** (g)
Q	1.73	63.3
H	1.617	63.4
T	1.845	60.5

Since the best performance results are achieved with the hexagonal core, further studies were developed having this geometry in mind. In order to calculate the displacements on the shelter, the equivalent stiffness of the sandwich structure was calculated and then applied to the simulations of the whole shelter with two pillars.

According to Shi [72], the Young's Modulus of a regular hexagonal core with uniform thickness, E_c, is given by

$$E_c = 2.3 \times E_h \left(\frac{t_h}{l_h}\right)^3 \tag{7.1}$$

where E_h is the Young's Modulus of the wall material, t_h is the thickness of the walls and l_h the length of the angled walls — see Figure 7.7.

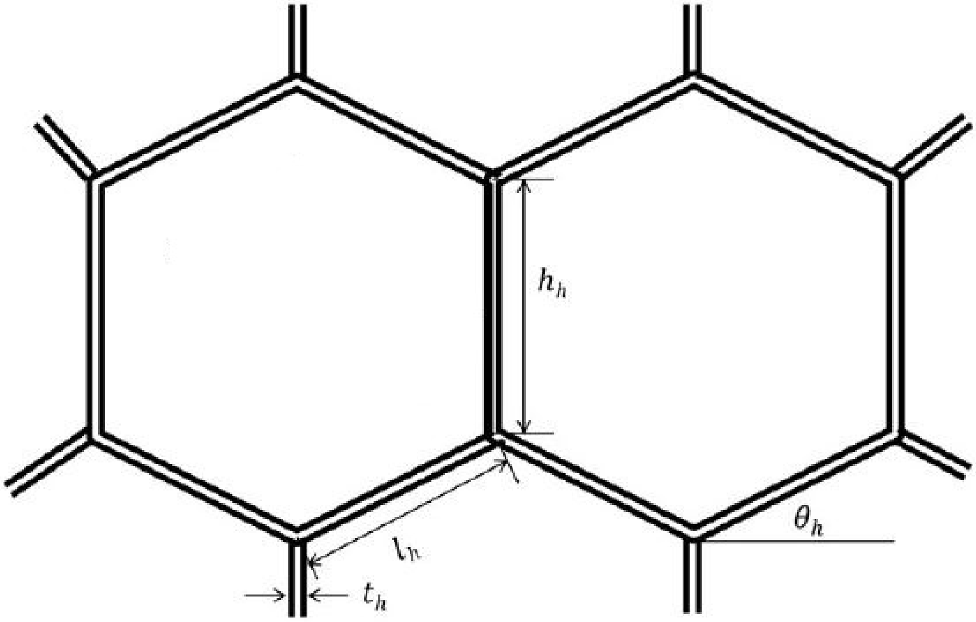

Figure 7.7 Geometry of hexagonal core [72].

The equivalent stiffness of the sandwich structure (which geometry is represented in Figure 7.8) is the sum of the bending stiffness of the hexagonal core and the two outer sheets [73]:

$$\begin{aligned}(EI)_{eq} &= E_c I_c + 2E_s I_s \\ &= E_c \frac{bc^3}{12} + E_s \left(\frac{bt^3}{6} + \frac{btd^2}{2} \right)\end{aligned}$$

Considering that the thickness of the sheets t is much smaller that the height of the core c and that the Young's Modulus, E_c (calculated in Equation (7.1)) is at least one order of magnitude smaller that E_s, the following simplification is reached [73]:

$$(EI)_{eq} = E_s \times \frac{btd^2}{2} \Leftrightarrow E_{eq} = \frac{E_s \times \frac{btd^2}{2}}{\frac{bd^3}{12}} = \frac{6 \times E_s \times t}{d}$$

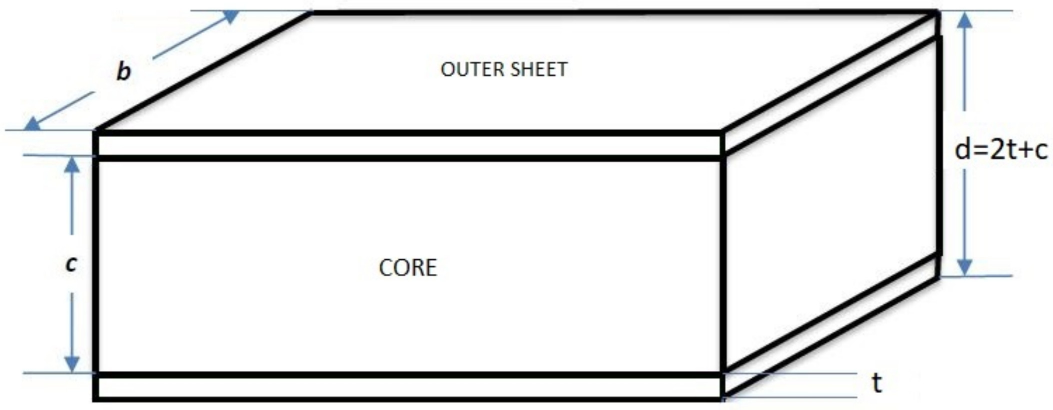

Figure 7.8 Geometry of sandwich structure.

These equations can be applied into the structure previously studied to choose the hexagonal core ($c = 5$ mm and $t = 0.5$ mm) and it results in a maximum displacement on the shelter of 419 mm (with a mass of 88 kg). It does not satisfy the requirements, but the combined results of maximum displacement and final mass have improved when compared to previous solutions. Table 7.7 shows some interesting examples of structures with a good performance. In ABAQUS ®, these results were obtained by altering the value of Young's Modulus to E_{eq} and the value of thickness, depending on the dimensions of each sandwich structure. All other parameters, such as the boundary conditions, the loads applied or the mesh, were maintained from previous simulations.

Table 7.7 Examples of sandwich structures and their respective maximum displacements of the shelter with two pillars.

Properties of structure	**Max. displacement on shelter** (mm)
$E_s = 2$ GPa, $c = 40\,mm$, $t = 2\,mm$	7.200
$E_s = 8$ GPa, $c = 40\,mm$, $t = 1.5\,mm$	8.970
$E_s = 20$ GPa, $c = 30\,mm$, $t = 1.5\,mm$	4.460

It should be noted that the calculation of the equivalent stiffness has an associated error, which means that, in the future, the shelter should be modelled with the sandwich structure and analysed in order to validate the results.

At this point, Table 7.7 proves that a sandwich structure can a reasonable solution for the shelter. Therefore, an experimental validation was performed in order to confirm whether the memory effect was still present, even with this kind of structure. Thus, a part was printed (Figure 7.9a) with a quadrangular infill as a 20 mm core. Afterwards, water was heated to the transition temperature. The part was submerged in water for a few seconds (Figure 7.9b), then deformed. When that deformation was fixed (Figure 7.9c), the part was submerged again and its initial shape was recovered (Figures 7.9d and 7.9e). This way, it can be concluded that this structure is valid to use in the application of this dissertation, since it maintains its shape memory effect.

In order to improve the results of Table 7.6, some dimensions of the sandwich structure can be varied: the thickness of the core, the thickness of the two extremity-sheets and the height of the core. For a better understanding of each of these parameters, Figure 7.10 shows a schematic representation of the dimensions mentioned relative to the core of the sandwich structure.

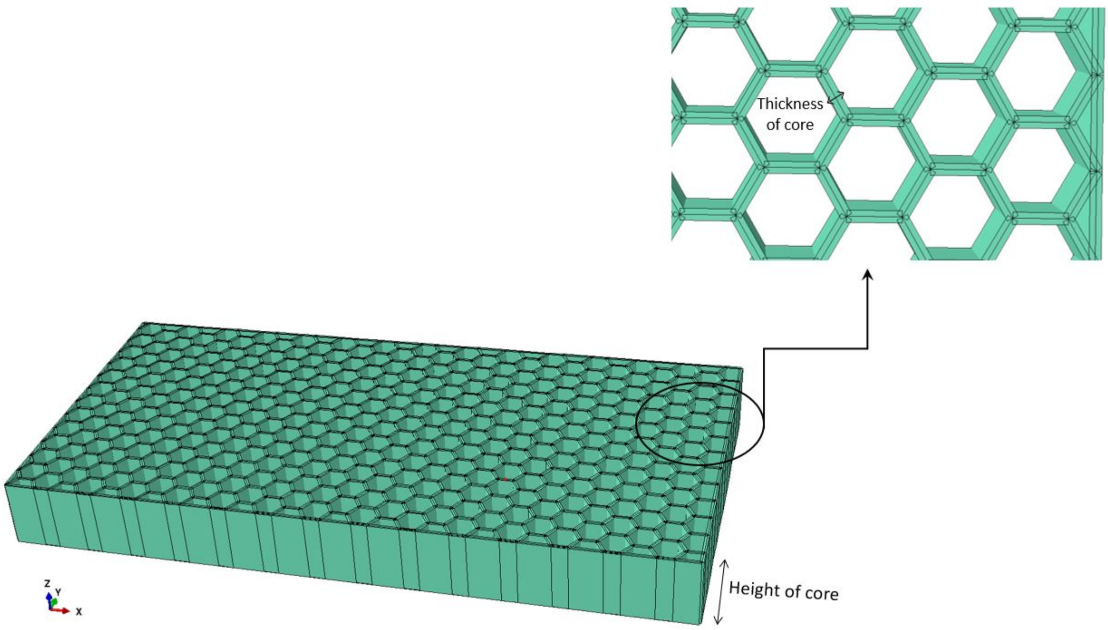

Figure 7.10 Parameters *thickness* and *height of core*.

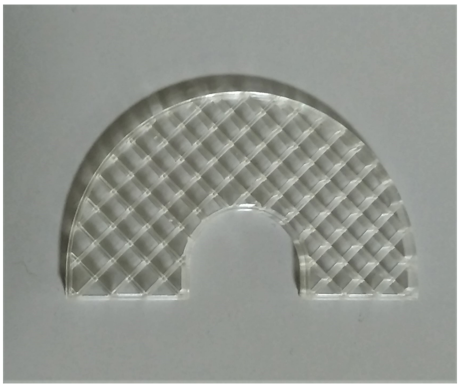

(a) Printed part.

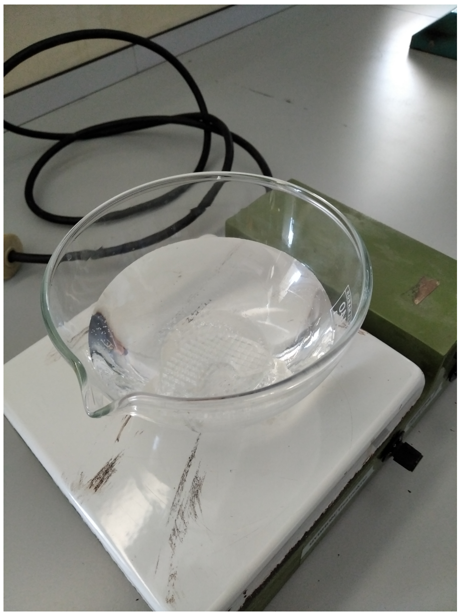

(b) Water heating and submersion of the part.

(c) Deformation imposed on the part.

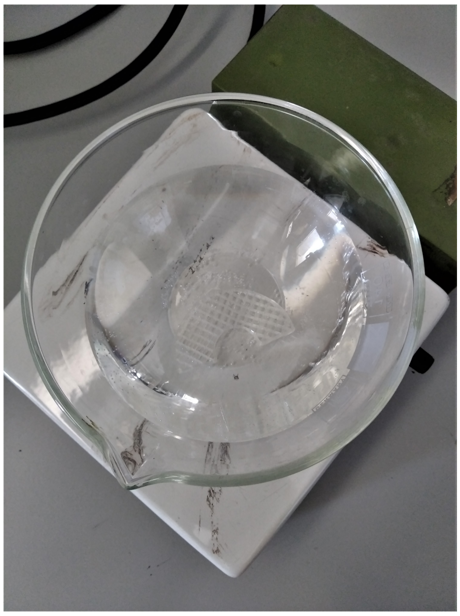

(d) Re-submersion of the part and return to the initial shape.

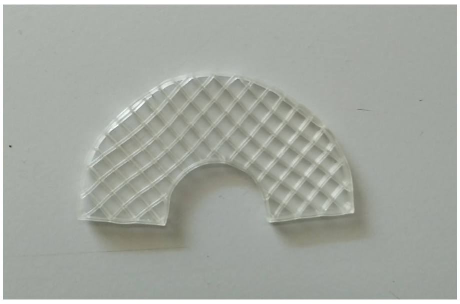

(e) Final part.

Figure 7.9 Practical experimentation for validation of shape memory effect on sandwich structure.

7.2 Sensitivity Analysis

With the goal of better understanding the influence of each parameter previously stated — thickness of the sheets, thickness and height of the core — on the performance of the structure, a sensitivity analysis was performed.

As described in Chapter 5, a Design Sensitivity Analysis (DSA) was performed on ABAQUS ® in which the derivatives of the three parameters with respect to the displacement were calculated. For that purpose, some modifications had to be made on the input file, such as the variation of the three design parameters and the activation of the DSA, as well as specifying the desired output variables. The results of the DSA performed are synthesized in Table 7.8. The sensitivities compared are the maximum values and show that small changes on the height of the core do not provoke big changes in the structure's stiffness. In addition, even though the values of the sensitivity of the two remaining design parameters are similar, the one related to the thickness of the outer sheets is higher, which means it has a bigger influence on the performance of the sandwich structure.

Table 7.8 Sensitivities obtained from the Design Sensitivity Analysis performed on ABAQUS ®.

Design Parameter	**Sensitivity**
Thickness of sheets	0.7173
Thickness of core	0.6812
Height of core	0.2669

In the attempt of validating these results, a more hands-on approach was performed, as several simulations with different changes of the design parameters were analysed and compared with respect to both maximum displacement and mass.

Table 7.9 Results obtained with changes of 20%.

Thickness of sheets (mm)	**Thickness of core** (mm)	**Height of core** (mm)	**Displacement** (mm)	Variation	**Mass** (kg)	Variation
0.5	1	20	0.1103		0.174	
0.5	1.2	20	0.1008	-0.0475[a]	0.204	015
0.6	1	20	0.09855	-0.1175	0.18	0.06
0.5	1	24	0.07757	-0.00818	0.204	0.0075

[a]The values of *Variation* shown in Tables 7.9 and 7.10 represent the difference of displacement or mass divided by the change in the design parameter. For instance, $\frac{0.1008-0.1103}{1.2-1} = -0.0475$.

Table 7.10 Results obtained with changes of 100%.

Thickness of sheets (mm)	**Thickness of core** (mm)	**Height of core** (mm)	**Displacement** (mm)	Variation	**Mass** (kg)	Variation
0.5	1	10	0.4488		0.1	
0.5	2	10	0.3537	-0.0951	0.174	0.074
1	1	10	0.2602	-0.3772	0.127	0.054
0.5	1	20	0.1103	-0.03385	0.174	0.0074

From the previous results, several conclusions can be discussed:

- the parameter *height of core* shows the smallest sensitivity, which means a small change in this parameter does not cause big differences on the structure's stiffness, which can be proven to be true by observing Table 7.11, that shows the displacement results when the design parameters are changed in 0.5 mm, which is a small variation for the parameter *height of the core*;

Table 7.11 Results obtained with changes of 0.5 mm.

Thickness of sheets (mm)	**Thickness of core** (mm)	**Height of core** (mm)	**Displacement** (mm)
0.5	1	20	0.1103
0.5	1.5	20	0.0983
1	1	20	0.07305
0.5	1	20.5	0.1051

- In terms of design, the parameters have different possible sizes. For instance, it is not physically possible to have the same value of thickness for the core and the sheets, due to the core's geometry. In addition, the value of sensitivity with respect to the mass also needs to be taken into consideration. In fact, the parameter that shows the smallest influence on the value of mass is *height of the core*.

- Because of the previous statement, bigger variations can be made on the height of the core without highly increasing the mass, but with much smaller displacements and, consequently, creating a stiffer structure. This can be proven by observing the absolute values of displacement on Tables 7.9 and 7.10 and confirming that the result relative to the variation of *height of the core* is the one that translates the best performance.

- Increasing the parameters *thickness of core* and *height of core* on the same proportion translates as an equal increase in mass. However, in this case, varying the *height of core* results in better performance (since it is a bigger variation). Furthermore, despite this result, the variation of *thickness of sheets* leads to lower mass.

Chapter 8

Conclusions and Future Work

Initially, the advantage of developing a fast-assembly shelter, without the need of any expertise, was immediately seen. It is crucial that temporary housing solutions are adequate to climatic loads, such as the wind, rain and snow, as so many displaced people have already lost their house, they shouldn't have poor conditions on a substitute one.

Shelters have a number of structural and design rules that need to be followed, being the most important one its rigidity, measured in terms of maximum displacement. Therefore, this dissertation focused on achieving a solution that was able to check that requirement, since the initial version of the shelter did not perform well.

During investigation for the dissertation, it was verified a lack of literature about the material used — DiAPLEX MM45-20 — and its behaviour when printed. Therefore, specimens were manufactured in three different directions and tested afterwards. It was concluded that printing with a direction of 0° results in parts with a higher Elastic Modulus (mean value of 2447 MPa).

When analysing the FEM results, the first conclusion was the need for pillars to strengthen the door opening. It is preferable that the pillars are made from the same material as the rest of the structure because the shelter can be manufactured at one go, by additive manufacturing.

The use of an interior reinforcement skeleton of supporting bars was considered. However, the added weight of the bars worsened the shelter's response. For this reason, the focus shifted to finding a rigid solution without much extra weight and so a sandwich structure was studied. A primitive study of this structure applied to a small plate was performed, which led to the the choice of studying an hexagonal core. By calculating the equivalent stiffness, this solution proved to be promising since the structural requirement of maximum displacement can be met. Hence, a sensitivity analysis was held in order to understand the influence of each geometric variable (thickness of core and sheets and height of core) on the rigidity and mass of the sandwich structure. The analysis showed that when varying the parameters in the same proportion, the variation of *height of the core* results in better performance, but higher mass. On the other hand, varying the parameter *thickness of sheets* results in the smallest influence on mass and second-best result in rigidity. Due to the sensitivity analysis, an optimization of the dimensions of the structure can be performed in the future to find the dimensions that possibilitate a shelter that meets both requirements: maximum displacement and mass.

All in all, using a sandwich structure in DiAPLEX MM545-20 with an hexagonal core can be the solution for the shelter in terms of stiffness, as well as of weight. Firstly, the sandwich structure should be modelled into the shelter in order to validate the values of displacement and mass calculated in this dissertation. If it is not possible to achieve acceptable values of mass, the solution can still be considered, as long as different loading conditions are examined (because the displacements will be much lower). In the future, instead of calculating the worse possible conditions, this study could be specialized having a specific place in mind, and, therefore, other loading conditions. Besides rethinking the loads, limiting this study to a part of the world means a seismic analysis could be performed, since it depends on the type of ground and seismic zone the country is included in. Additionally, this dissertation only focus on European countries, even though it is known several non-European countries that would benefit from better housing solutions.

In order to decrease the mass of the shelter, and consequently its cost, topology optimization could be considered. Another interesting approach would be to implement a shape memory foam as the core of the sandwich structure.

When a good solution is achieved, it is also recommended that a more in-depth finite element analysis is done, such as introducing anisotropic properties of the material and a folding/unfolding simulation.

Lastly, a deeper economical analysis should be performed, since one of the issues with the initial version of the shelter is its high cost and adding more material so the shelter becomes stiffer results in even higher cost.

References

[1] L. A. C. Henriques, "4D Structures for Rapid Construction of a Shelter in Crisis Situations," MSc thesis, University of Porto, 2019.

[2] S. Krishnan and Y. Liao, "Integrating Shelter Design and Disaster Education in Architectural Curriculum," in *126th Annual Conference and Exposition - American Society for Engineering Education*, 2019.

[3] E. A. Peraza-Hernandez, D. J. Hartl, and R. J. Malak Jr, "Design and numerical analysis of an SMA mesh-based self-folding sheet," *Smart Materials and Structures*, vol. 22, no 9, page 94008, 2013, doi: 10.1088/0964-1726/22/9/094008.

[4] E. A. Peraza-Hernandez, D. Hartl, E. Akleman, and K. Frei, "Connectivity of Shape Memory Alloy-based Self-Folding Structures," in *22nd AIAA/ASME/AHS Adaptive Structures Conference*, jan 2014, doi: 10.2514/6.2014-1415.

[5] G. Curletto and L. Gambarotta, "Rigid foldable origami structures: integrated parametric design and structural analysis," in *International Association for Shell and Spatial Structures Symposium*, 2015.

[6] J. O'Neil, A. A. Deleo, H. Yasuda, M. Salviato, and J. Yang, "Deployable Structures Constructed from Composite Origami," in *33th ASC conference*, Seattle, jul 2018, doi: 10.12783/asc33/25907.

[7] N. de Temmerman, K. Roovers, L. A. Mira, A. Vergauwen, A. Koumar, S. Brancart, L. D. Laet, and M. Mollaert, "Lightweight transformable structures: materialising the synergy between architechtural and structural engineering," *WIT Transactions on The Built Environment*, vol. 136, 2014.

[8] L.-G.-A. Rhode-Barbarigos, "An Active Deployable Tensegrity Structure," Ph.D. dissertation, École Polytechnique Fédérale de Lausanne, 2012.

[9] N. D. Temmerman and L. A. Mira, "Deployable scissor arch for transitional shelters," *Automation in Construction*, 2014.

[10] D. Vaughn, A. Smith, B. Tower, G. Hummel, J. Dooley, and S. Li, "Origami Emergency Shelter," Tech. Rep., dec 2019, doi: 10.13140/RG.2.2.28594.56007.

[11] J. Pable, "Shelter design can help people recover from homelessness," 2018. [Online]. Available: https://www.engineeringforchange.org/news/shelter-design-can-help-people-recoverhomelessness/ [Accessed Feb. 23, 2020].

[12] International Organization for Migration, “Shelter and non-food items,” in *Emergency Manual*.

[13] ——, “About IOM: Mission.” [Online]. Available: https://www.iom.int/mission [Accessed Mar. 28, 2020].

[14] ——, “IOM in Shelter.” [Online]. Available: https://www.iom.int/shelter [Accessed Mar. 28, 2020].

[15] I. F. of Red Cross, “About IFRC.” [Online]. Available: https://media.ifrc.org/ifrc/ [Accessed Mar. 26, 2020].

[16] I. F. o. R. C. Societies and R. Crescent, *The IFRC shelter kit*. IFRC, 2009.

[17] S. Association, *The Sphere Handbook: Humanitarian Charter and Minimum Standards in Humanitarian Response*, 4th ed., Geneva, Switzerland, 2018. [Online]. Available: www.spherestandards.org/handbook

[18] A. Bashawri, S. Garrity, and K. Moodley, “An Overview of the Design of Disaster Relief Shelters,” in *4th International Conference on Building Resilience*, Salford Quays, 2014.

[19] I. F. o. R. C. Societies and R. Crescent, *Transitional Shelters - Eight designs*, Geneva, 2011.

[20] A. V. Nasser, “Development of a Light Weight Structure Emergency Housing of Refugees,” Ph.D. dissertation, Chalmers University of Technology, 2011.

[21] U. N. H. C. for Refugees, “Framed Tent,” 2014, uNHCR Item No 06642.

[22] G. Gardiner, “Composites in tornado shelters,” 2016. [Online]. Available: https://www.compositesworld.com/blog/post/composites-in-tornado-shelters [Accessed Feb. 25, 2020].

[23] S. Francis, “FRP, pultrusion enable mobile Antarctic habitat module,” 2019. [Online]. Available: https://www.compositesworld.com/blog/post/frp-pultrusion-enable-mobile-antarctic-habitat-module

[24] Cardorigami, “Cardborigami.” [Online]. Available: https://www.cardborigami.org/ [Accessed Mar. 26, 2020].

[25] Designboom, “Designnobis’ tentative provides shelter in post-disaster situations.” [Online]. Available: https://www.designboom.com/design/designnobis-tentative-post-disaster-shelter-07-11-2015/ [Accessed Mar. 26, 2020].

[26] P. Lynch, “Barberio Colella ARC Designs Pop-Up Home to Rebuild Nepalese Lives in "Just a Minute".” [Online]. Available: https://www.archdaily.com/775698/barberio-colella-arc-designs-pop-up-home-to-rebuild-nepalese-lives-in-just-a-minute [Accessed Mar. 26, 2020].

[27] Z. G. Hasan, “Inexpensive, Easy-to-Build Gridshell Pavilion Uses Air-Filled Cushions for Construction.” [Online]. Available: https://www.archdaily.com/880694/inexpensive-easy-to-build-gridshell-pavilion-uses-air-filled-cushions-for-construction [Accessed Mar. 26, 2020].

[28] SO?, “FOLDFLOAT.” [Online]. Available: https://www.soistanbul.com/fold-float-1 [Accessed Mar. 26, 2020].

[29] Archello, “Weaving A Home.” [Online]. Available: https://archello.com/project/weaving-a-home [Accessed Mar. 26, 2020].

[30] T. M. Architecture and D. Workshop, “Shelter Squared.” [Online]. Available: http://madworkshop.org/projects/shelter-squared/ [Accessed Mar. 26, 2020].

[31] M. Tent, “Maidan Tent.” [Online]. Available: https://www.maidantent.org/ [Accessed Mar. 26, 2020].

[32] X. Xin, L. Liu, Y. Liu, and J. Leng, “Mechanical Models, Structures, and Applications of Shape-Memory Polymers and Their Composites,” *Acta Mechanica Solida Sinica*, vol. 32, no 5, pages 535–565, 2019, doi: 10.1007/s10338-019-00103-9.

[33] W. Liu, “Material Design for 3D Printing of Environmentally Responsive Composites and Structures,” Ph.D. dissertation, Stevens Institute of Technology, 2019.

[34] F. Momeni, S. M. Mehdi, H. N., X. Liu, and J. Ni, “A review of 4D printing,” *Materials and Design*, vol. 122, pages 42–79, 2017.

[35] Z. Zhang, K. G. Demir, and G. X. Gu, “Developments in 4D-printing: a review on current smart materials, technologies, and applications,” *International Journal of Smart and Nano Materials*, vol. 10, no 3, pages 205–224, 2019.

[36] Y. Mao, K. Yu, M. S. Isakov, J. Wu, M. L. Dunn, and H. Jerry Qi, “Sequential Self-Folding Structures by 3D Printed Digital Shape Memory Polymers,” *Scientific Reports*, vol. 5, no 1, page 13616, 2015, doi: 10.1038/srep13616.

[37] W. Wang, H. Rodrigue, and S.-H. Ahn, “Deployable Soft Composite Structures,” *Scientific Reports*, vol. 6, feb 2016, doi: 10.1038/srep20869.

[38] P. Mather, X. Luo, and I. Rousseau, “Shape Memory Polymer Research,” *Annu. Rev. Mater. Res*, vol. 39, pages 445–471, aug 2009.

[39] C. A. Garcia Rosales, H. Kim, M. F. G. Duarte, L. Chavez, M. Castañeda, T.-L. B. Tseng, and Y. Lin, “Characterization of shape memory polymer parts fabricated using material extrusion 3D printing technique,” *Rapid Prototyping Journal*, 2018.

[40] S. Liu and Q.-S. Yang, "Finite element analysis of shape-memory polymer mast," *International Journal of Smart and Nano Materials*, vol. 10, no 4, pages 285–299, 2019, doi: 10.1080/19475411.2019.1686666.

[41] S. T. Inc., "SMP Tech 20E-Catalogue: Intelligent Material," Tech. Rep., 2018.

[42] Q. Zhao, H. J. Qi, and T. Xie, "Recent progress in shape memory polymer: New behavior, enabling materials, and mechanistic understanding," *Progress in Polymer Science*, vol. 49-50, pages 79–120, oct 2015, doi: 10.1016/J.PROGPOLYMSCI.2015.04.001.

[43] J. Gu, J. Leng, H. Sun, H. Zeng, and Z. Cai, "Thermomechanical constitutive modeling of fiber reinforced shape memory polymer composites based on thermodynamics with internal state variables," *Mechanics of Materials*, vol. 130, pages 9–19, mar 2019. [Online]. Available: https://www.sciencedirect.com/science/article/pii/S0167663618302862

[44] S. Joshi, K. Rawat, K. C, V. Rajamohan, A. T. Mathew, K. Koziol, V. Kumar Thakur, and B. A.S.S, "4D printing of materials for the future: Opportunities and challenges," *Applied Materials Today*, vol. 18, page 100490, 2020, doi: 10.1016/j.apmt.2019.100490.

[45] P. R. Buckley, G. H. McKinley, T. S. Wilson, W. Small IV, W. J. Bennett, J. P. Bearinger, M. W. McElfresh, and D. J. Maitland, "Inductively Heated Shape Memory Polymer for the Magnetic Actuation of Medical Devices," Department of Mechanical Engineering, Massachusetts Institute of Technology, Tech. Rep., 2006.

[46] M. Sáenz-Pérez, T. Bashir, J. M. Laza, J. García-Barrasa, J. L. Vilas, M. Skrifvars, and L. M. León, "Novel shape-memory polyurethane fibers for textile applications," *Textile Research Journal*, 2018.

[47] S. T. Inc., "SMP Filament," Tech. Rep.

[48] European Comittee for Standardization, "Plastics - Determination of tensile properties - Part 2: Test conditions for moulding and extrusion plastics - BS EN ISO 527-2:1996," pages 1–14, 1996.

[49] D. C. Montgomery, *Introduction To Statistical Quality Control*, 6th ed. Arizona: John Wiley & Sons, Inc., 1985, vol. 10.

[50] T. Mu, L. Liu, X. Lan, Y. Liu, and J. Leng, "Shape memory polymers for composites," *Composites Science and Technology*, vol. 160, pages 169–198, may 2018, doi: 10.1016/J.COMPSCITECH.2018.03.018.

[51] B. Goo, C.-H. Hong, and K. Park, "4D printing using anisotropic thermal deformation of 3D-printed thermoplastic parts," *Materials & Design*, vol. 188, page 108485, mar 2020. [Online]. Available: https://www.sciencedirect.com/science/article/pii/S0264127520300186

[52] D. K. Verma, R. Purohit, R. Rana, S. Purohit, and K. Patel, “Enhancement of the properties of shape memory polymers using different nano size reinforcement – A review,” *Materials Today: Proceedings*, mar 2020, doi: 10.1016/J.MATPR.2020.02.631.

[53] G. Sossou, F. Demoly, H. Belkebir, H. J. Qi, S. Gomes, and G. Montavon, “Design for 4D printing: A voxel-based modeling and simulation of smart materials,” *Materials & Design*, vol. 175, page 107798, aug 2019. [Online]. Available: https://www.sciencedirect.com/science/article/pii/S0264127519302357

[54] H. S. V., M. D. Hoang, J. F. Simpson, and T. H. Kwok, “4D Printing of Composites,” in *21st International Conference on Composite Materials*, Xi’an, 2017.

[55] S. H. Masood, *Advances in Fused Deposition Modeling.* Elsevier, 2014, vol. 10, doi: 10.1016/B978-0-08-096532-1.01002-5.

[56] Y. Yang, Y. Chen, Y. Wei, and Y. Li, “3D printing of shape memory polymer for functional part fabrication,” *The International Journal of Advanced Manufacturing Technology*, vol. 84, sep 2015.

[57] B. Rupal, K. Mostafa, Y. Wang, and A. J. Qureshi, “A Reverse CAD Approach for Estimating Geometric and Mechanical Behavior of FDM Printed Parts,” *47th SME North American Manufacturing Research Conference*, vol. 34, pages 535–544, 2019.

[58] T. Chartier and A. Badev, *Rapid Prototyping of Ceramics*, 2nd ed. Elsevier, 2013, doi: 10.1016/B978-0-12-385469-8.00028-9.

[59] T. Liu, L. Liu, C. Zeng, Y. Liu, and J. Leng, “4D printed anisotropic structures with tailored mechanical behaviors and shape memory effects,” *Composites Science and Technology*, vol. 186, page 107935, jan 2020. [Online]. Available: https://www.sciencedirect.com/science/article/pii/S0266353819314964

[60] J. N. Reddy, *An Introduction to the Finite Element Method*, 3rd ed. Texas: McGraw-Hill, 2006.

[61] D. Systemes, “Abaqus/CAE.” [Online]. Available: https://www.3ds.com/products-services/simulia/products/abaqus/abaquscae/ [Accessed Mar. 26, 2020].

[62] E. Oñate, *Structural Analysis with the Finite Element Method. Linear Statics. Volume 2. Beams, Plates and Shells*, 1st ed. Barcelona: Springer, 2013.

[63] G. R. Liu and S. S. Quek, *The Finite Element Method: A Practical Course.* Singapore: Butterworth-Heinemann, 2003.

[64] F. Teixeira-Dias, J. P. da Cruz, R. A. F. Valente, and R. J. A. de Sousa, *Método dos Elementos Finitos: Técnicas de Simulação Numérica em Engenharia*, 1st ed. LIDEL, 2009.

[65] G. P. Nikishkov, “Introduction to the finite element method,” 2004, lecture Notes, University of Aizu.

[66] Q. Guo and A. E. Jeffers, “Direct differentiation method for response sensitivity analysis of structures in fire,” *Engineering Structures*, vol. 77, pages 172–180, 2014, doi: 10.1016/j.engstruct.2014.06.025.

[67] T. Haukaas, “Efficient computation of response sensitivities for inelastic structures,” *Journal of Structural Engineering*, vol. 132, no 2, pages 260–266, 2006, doi: 10.1061/(ASCE)0733-9445(2006)132:2(260).

[68] E. Commission, “EN Eurocode Parts.” [Online]. Available: https://eurocodes.jrc.ec.europa.eu/ [Accessed Mar. 25, 2020].

[69] C. E. de Normalização, “Eurocódigo - Bases para o projeto de estruturas,” Standard, 2009.

[70] T. E. S. P. C. Group, *Structural Design of Polymer Composites: EUROCOMP Design Code and Handbook*, J. L. Clarke, Ed., 1996, doi: 10.1017/CBO9781107415324.004.

[71] J. Acacio, “Análise do comportamento a flexão em sanduíches com núcleos impressos em 3D,” Faculdade de Engenharia da Universidade do Porto, Porto, Tech. Rep., 2020.

[72] S. Shi, B. Chen, and Z. Sun, “Equivalent properties of composite sandwich panels with honeycomb–grid hybrid core,” *Journal of Sandwich Structures and Materials*, vol. 22, 07 2018, doi: 10.1177/1099636218789615.

[73] J. Gryzagoridis, G. Oliver, and D. Findeis, “On the equivalent flexural rigidity of sandwich composite panels,” *Insight - Non-Destructive Testing and Condition Monitoring*, vol. 57, 03 2015, doi: 10.1784/insi.2014.57.3.140.

Appendix A

Technical drawing of the initial structure [1]

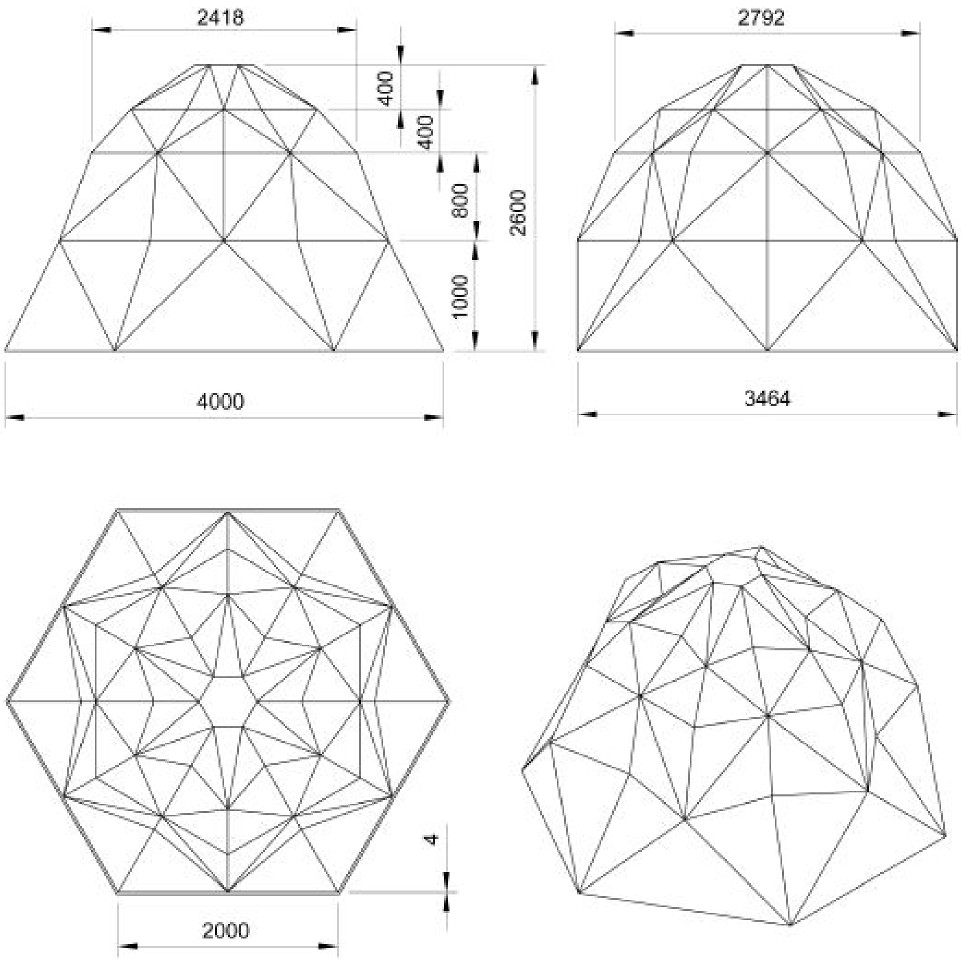

Structure study model	June 2019
Alice Costa	**Scale 1:50**

Appendix B

Technical drawing of the initial structure with door opening [1]

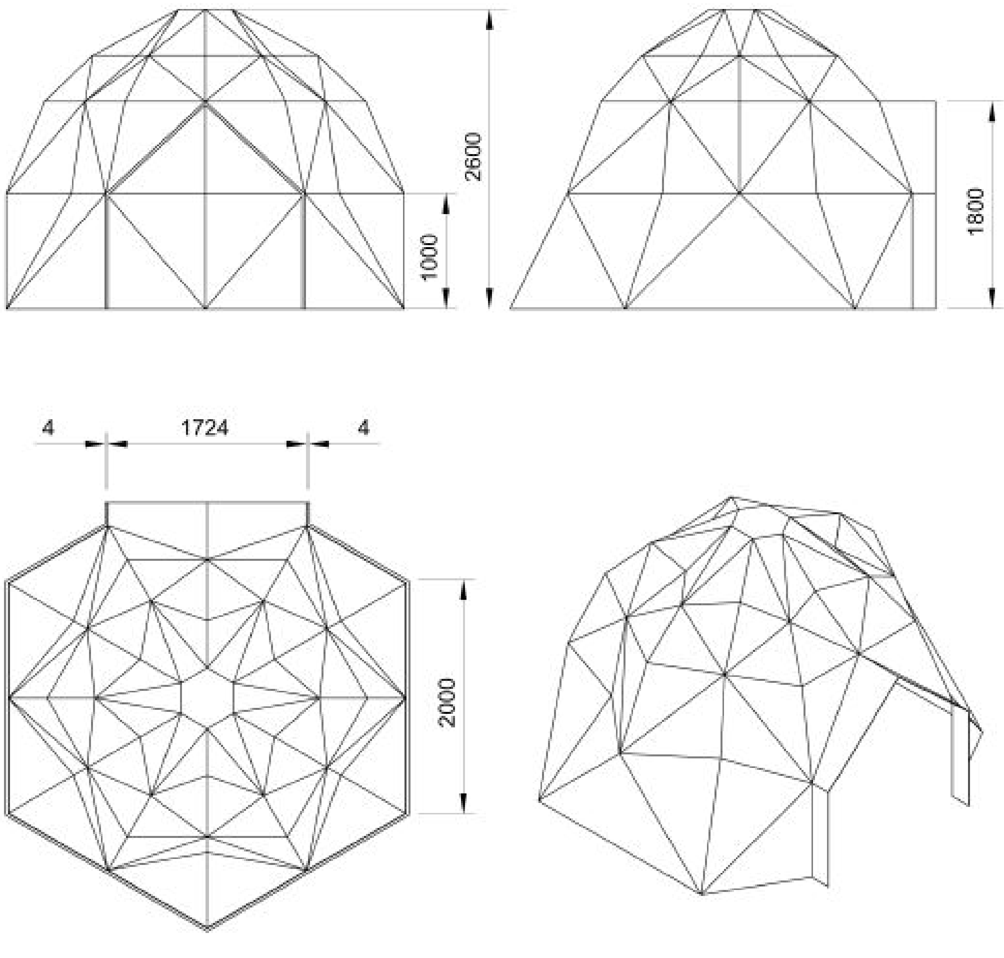

Model with door opening	June 2019
Alice Costa	**Scale 1:50**

Appendix C

Technical drawing of the initial structure with 2 openings (expansion) [1]

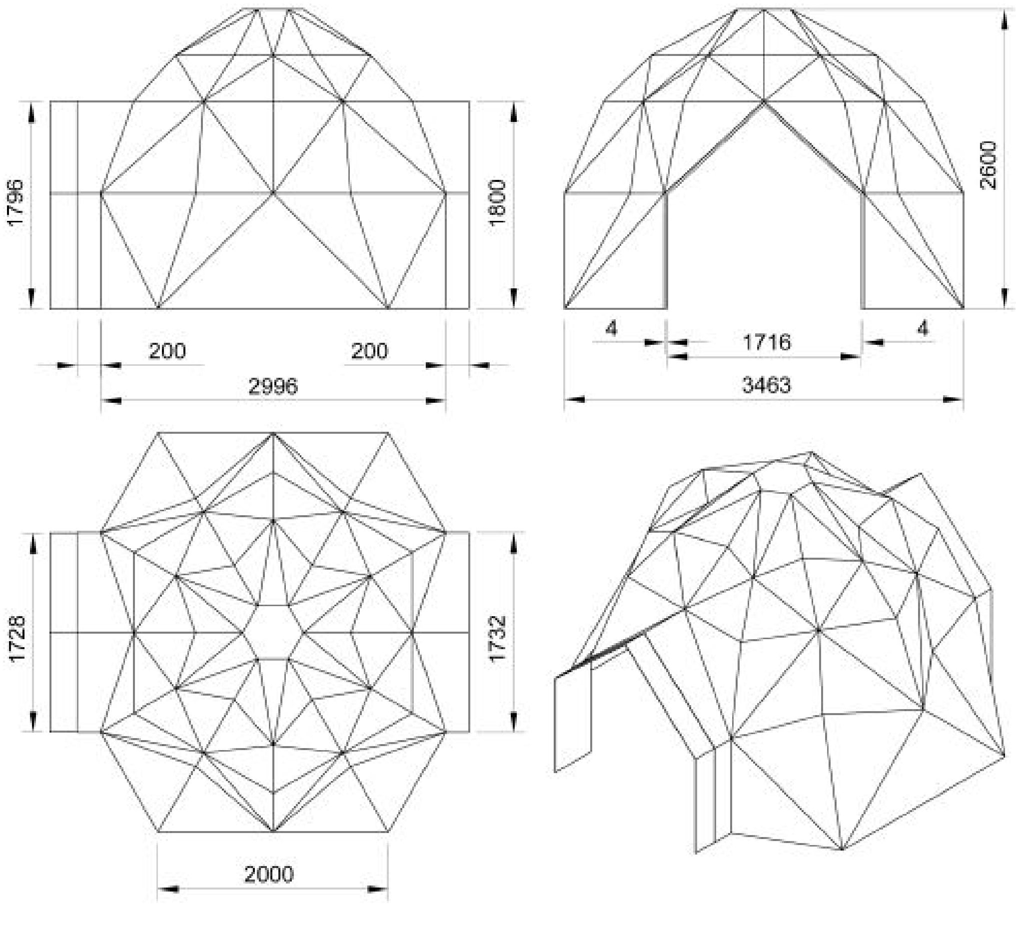

Model with two openings for connection	June 2019
Alice Costa	**Scale 1:50**